JET PENETRATION DEPTH MEASUREMENTS AND AXIAL-FLOW PROPELLER PUMP RE-CALIBRATION IN A STRATIFIED MEDIUM

By

HOWELLS IDAEREFAGHA HART II

Bachelor of Engineering

University of Benin

Benin-City, Nigeria

1977

Submitted to the Faculty of the Graduate College
of the Oklahoma State University
in partial fulfillment of the requirements
for the Degree of
MASTER OF SCIENCE
July, 1981

JET PENETRATION DEPTH MEASUREMENTS AND AXIAL-FLOW PROPELLER PUMP RECALIBRATION IN A STRATIFIED MEDIUM

Thesis Approved:

J. W. Morrell
Thesis Adviser

D. K. McLaughlin

David G. Lilley

Norman N. Durham
Dean of Graduate College

ACKNOWLEDGMENTS

The author's respect and appreciation to his major adviser, Dr. Peter M. Moretti, for his guidance and assistance which made this study a success, go beyond that which formality requires. His readiness to help even in matters not directly related to this study is gratefully acknowledged. Appreciation is also expressed to the other members of my committee, Dr. D. K. McLaughlin and Dr. D. G. Lilley for their criticism and advice which helped produce a more comprehensible and authentic report.

A note of thanks is given to the Department of Mechanical and Aerospace Engineering for the research assistantship and facilities provided. It is worth mentioning that the project was funded by a grant from the Waterway Experiment Station in Vicksburg, Mississippi.

Thanks are also extended to my Christian brothers and sisters who persevered with me in prayers throughout this study. To God be the glory. Special appreciation goes to my parents Mr. and Mrs. E. B. Hart who had always been of much support.

Very special gratitude goes to my wife, Faustina, for her understanding, encouragement and sacrifices especially prior to and immediately after the birth of our son, Sofiri, when I spent long hours into the nights out in the laboratory and much of Sofiri's essential services had to be rescheduled. Dedicating this thesis to them is only a poor way of showing that I highly appreciated it all.

TABLE OF CONTENTS

TABLE

LIST OF FIGURES

NOMENCLATURE

A_m	Area of the model
A_p	Area of the propeller
A_{pr}	Area of prototype
D	Distance between camera and propeller shaft
d	Distance between camera and side of basin
D_p	Propeller diameter
DF	Dilution Factor
DO	Dissolved oxygen
F_R	Pumping Force
Fr	Froude number, $Fr = V/(gh)^{1/2}$
Fr_d	Densimetric Froude number, $Fr_d = V/\ g(\Delta\rho/\rho_o)h^{1/2}$
g	Gravitational constant
g'	Effective gravitational constant, $g' = g\ (\Delta\rho/\rho_o)$
H	Total depth of basin
h^*_{po}	Non-dimensional difference from propeller depth to any point, P
h_o	Propeller depth measured from the surface
h_o^*	Non-dimensional Propeller depth, $h_o^* = h_o/D_p$
h_s	Penetration depth measured from the surface
h_s^*	Non-dimensional penetration depth, $h_s^* = h_s/D_p$
h_t	Thermocline location measured from the surface
h_t^*	Non-dimensional thermocline location, $h_t^* = h_t/D_p$
h_{so}	Propeller depth to penetration depth, $h_{so} = h_s - h_o$

h_{so}^*	Non-dimensional propeller depth to penetration depth, $h_{so}^* = (h_s - h_o)/D_p$
h_{st}	Thermocline to stagnation point, $h_{to} = h_t - h_o$
h_{st}^*	Non-dimensional Thermocline location to stagnation point, $h_{st}^* = (h_s - h_t)/D_p$
h_{to}	Propeller depth to thermocline, $h_{to} = h_t - h_o$
h_{to}^*	Non-dimensional propeller depth to thermocline, $h_{to}^* = (h_t - h_o)/D_p$
K	Constant
L_1	h_{to}
L_m	Length in the model
L_o	Distance from propeller to plate
L_{pr}	Length in the prototype
L_r	Length ratio, $LR = L_{pr}/L_m$
Q_a	Actual flowrate
Q_e	Effective flowrate, $Q_e = \omega \cdot \gamma_p \cdot A_p$
Q_i	Ideal flowrate
Q_m	Flowrate in the model
Q_{pr}	Flowrate in the prototype
$Q_{p_{th}}$	Theoretical propeller flowrate
R	Distance from propeller shaft to dye streak at time = t
r	Distance from propelelr shaft to dye streak at time = t + ΔT, radius.
$\bar{r}$, $\bar{R}$	Axtual distances
$\bar{r}'$, $\bar{R}'$	Observed $\bar{r}$, $\bar{R}$ from film
r_p	Propeller radius, $r_p = D_p/2$
Ri	Richardson number, $Ri = g\Delta\rho/\rho_o \cdot L/V^2$
S	Actual grid spacing
S_o	Observed grid spacing

U	Velocity of a blade at a given radius, $U = \omega \cdot \gamma_p$
V_o	Average axial velocity through the propeller
W	Weight
X	Actual Distance
X'	Observed X from film
Z_p	Penetration depth measured from the surface
Z_p^*	Non-dimensional penetration depth, $Z_p^* = Z_p/H$
Z_T	Metalimnion location measured from the bottom
Z_T^*	Non-dimensional metalimnion location, $Z_T^* = Z_T/H$

Greek Letters

β	Blade angle
$\bar{\delta}$	Average specific weight
Δ	Difference
ρ	Density
ω	Rotational speed
η	Efficiency
θ	Angle of entrainment
$\Delta\rho/\rho_o$	Stratification

Subscripts

a	axial
d	densimetric
e	effective
i	incremental
m	model
o	propeller position

p	propeller, any point
s	stagnation point
t	thermocline

CHAPTER I

INTRODUCTION

Background

Seasonal heating and cooling of a body of water can give rise to the formation of layers of water with different densities. In the winter, the water in a reservoir is virtually of uniform density. Constantly cooled top water convects down to be replaced by the water from the bottom as the density of the former increases over the latter. This process provides comparatively good mixing until the hot months set in. At the advent of the hot months, the top water is warmed and a layer of warmer water is formed over the colder water of the bottom. A natural means of continued mixing is the wind. When this is not enough to completely mix the reservoir, a density gradient results.

The top layer, which is kept well mixed by the wind and therefore is richer in dissolved oxygen, is called the epilimnion. At the bottom of the epilimnion, where wind effects and mixing become minimal, the metalimnion or thermocline begins. This is a transition zone of rapidly decreasing temperature. Below the thermocline, isolated from the surface induced mixing effects, the bottom layer called the hypolimnion is formed. The hypolimnion is a low temperature and frequently oxygen-depleted layer (Figure 1). Through depletion of oxygen in the hypolimnion, anaerobic conditions may result, chemical reduction

processes may occur, and high concentrations of toxic materials may be formed.

Unfortunately, many of the older dams in the USA have their release gates located at the bottom of the reservoir and they release low quality water.

Artificial destratification, localized mixing and the modifications of the release gates of the dams are some of the ways that can be used to improve the quality of water. Artificial destratification can be done either by pumping compressed air near the bottom and letting it rise to produce a mixing effect, or by mechanically pumping the lower water to the surface, but requires high energy consumption and is complicated (22), (24). Structural modification of dams by relocating the release gates close to the top may be effective but is also very costly.

Quintero and Garton (19) came out with a low-energy axial-flow propeller pump that mixed the epilimnion water with the hypolimnium by the downward movement of a jet. This simple device consists essentially of a six-bladed 72 inch (1.83 m) Acme Windmaster fan (Figure 2), capable of producing a flow of 1.8 m^3/sec at 19.1 rpm. The propeller pump has been used in a number of places such as Lake Okatibee, Mississippi (10), and there has been considerable study at Oklahoma State University (6), (11), (12), (13), (14), (17), (18), (21), (22), (26) on various aspects of flow in a stratified lake and the performance of the Garton pump. The present study is a continuation on the performance of the propeller pump.

Related Research

A number of research projects have been carried out on the behavior of jets issuing into a density stratified medium. Baines (2), (3) studied the rate of entrainment of a plume or jet impinging on a density interface. He concluded that the entrainment flux into the plume is a function of the densimetric Froude number, Fr_d. Ditmars (8) investigated the mixing of density stratified impoundments by buoyant jets. He came up with a simulation technique to predict the changes that occur in the density profile of an impoundment during mixing. Abraham and Eysink (1) examined the case of jets issuing vertically upwards into fluids with density gradient. They came up with a theoretial analysis for determining the maximum upward penetrations of such jets. Givens (12) did a hydraulic model study of the local destratification phenomenon using Garton type propeller pumps. He concluded that for increasing values of the Richardson number, R_i, the penetration depth Z_p decreases. Moon (14) did a similar study. Busnaina (6) did a numerical simulation of the flow field of the jet induced by an axial-flow propeller pump by solving the governing equations of the flow field. He suggested an empirical expression for predicting the penetration depth.

Analytical derivations of the penetration depth of a jet moving through a stratified medium have been produced by a good number of persons. Three of such derivations are shown in Appendix C.

Objectives

The main objectives of this study are:

1. To prove the validity of the theoretical analysis of the propeller jet penetration depth in a stratified medium.
2. Depending on the outcome of (1) above, to develop an empirical relationship between the propeller velocity in the axial direction and the jet penetration depth in a stratified medium, and to re-calibrate the propeller as needed.

CHAPTER II

EXPERIMENTAL APPARATUS

Basin and Pumping Unit

The basin in which the experiments were performed is a rectangular tank that measures 4 ft. x 8 ft. x 3 ft. It is constructed with plexiglass about 1/2 inch thick and it is braced along the sides to give the structure more strength. The principal reason for making it of plexiglass is to ensure that an observer sees the mixing process during an experiment. The basin stands on supports about 2 ft. high; and to ensure easy access to it, a platform equally high is provided.

A separate tank which stands on the floor is used for the actual mixing of the salt solutions to specific densities. The mixing tank and the basin are equipped with a plumbing system that makes it possible for the salt solution to be pumped from the former to the later. The salt solution is first pumped to a reservoir tank which rest on a platform about 8 ft. high and from there into the basin.

An essential part of the experiment is the pumping of the salt solution into the basin without having it mix with the fresh water. To help accomplish this, the plumbing from the reservoir to the basin ends in a finely perforated "lip" which rests very close to the floor of the basin. A photograph of the test basin is shown in Figure 4.

Propeller and Driving Mechanism

A 4 1/2 inch (0.114 m) propeller model was used in this study. It is a model of the 72 inch, six-bladed Garton Pump shown in Figure 2. The propeller has a blade angle of 60 degrees at the hub and 25 degrees at the tip.

The driving mechanism consists of a 0-12 volts DC motor and a pulley arrangement that drives the propeller shaft. The propeller rotational speed is monitored with a digital counter through a magnetic pickup on the propeller shaft. A Hasler tachometer has also been used. The propeller speed is adjusted by varying the voltage across the motor. A tiny pipe through which dye solution flows from a sump ends just above the propeller.

Conductivity Unit

Electrical conductivity is a function of the salinity of water and since the density of water is a function of its salinity, electrical conductivity can be used as an indicator of the density of water.

The conductivity unit is made up of the conductivity probe, a hydrometer (specific gravity 1.000-1.010) and ten calibration samples of salt solutions of densities varying from 1.000 to 1.020. The main feature of the probe is its platinum black coating of the tips of the legs. A schematic drawings of the conductivity unit and the complete laboratory facility are shown in Figure 5 and Figure 6 respectively.

CHAPTER III

EXPERIMENTAL METHODS AND PROCEDURES

Calibrating the conductivity probe and stratifying the basin are normally done before any penetration experiment is carried out.

Coating the Conductivity Probe

The calibration of the probe relates the electrical resistance (ohms) experienced across the legs of the probe to the density of the salt solution the probe dips into. The resistance in any given solution depends on how good the platinum black coating is, increasing as the coating wears off.

To make the solution for the coating, 0.3 gm of platinum chloride, 0.006 gm of lead acetate and 20 cc of water are mixed. Mixtures could also be made with similar ratios of the items. The probe is dipped into a beaker of the coating solution with its tips well covered by the solution. The other end of the probe is connected through the wire terminals to a D-C power source and the voltage is adjusted to read between 3 and 5 volts.

About thirty seconds after the power is turned on, platinum black coatings appear on the probe tips and the probe terminals connected to the supply are interchanged. The interchanging process is repeated about every thirty seconds until good black coatings appear on both tips of the probe. The power is then switched off and the probe is

cleaned by dipping it in distilled water for a while. It is later brought out, left to dry and is then ready for use.

Calibrating the Probe

To calibrate the probe its terminals are connected to a digital multimeter which is set to read resistance. The probe tips are dipped into the salt solution samples and for each sample the corresponding resistance is read from the multimeter. A plot of resistance against specific gravity gives the calibration curve of the probe for that particular calibration.

The probe coating deteriorates when it is left in salt solution for a total period of about thirty minutes and if such a probe is calibrated a calibration curve very much different from the one with good coating is obtained. Also, different solution temperatures yield different curves but this was not much of a problem because the room temperature for a particular period did not change enough to cause any variations of the curves. To ensure that a curve obtained at the start of an experiment has not changed during an experiment, quick checks are made from time to time. The probe is recoated each time the resistances in the solution samples go higher than five percent of the original values. Figure 7 shows a typical calibration curve.

Stratifying the Basin

A density profile is first defined and this is fixed by the location of the metalimnion. All through the experiments a total height of 20 inches (0.508 m) was maintained.

Fresh water is pumped directly into the basin to the desired

height and is left to attain the room temperature. Salt solution is prepared in the mixing tank by dissolving non-iodized common salt (NaCl) in fresh water until the required density is attained. The specific gravity used throughout the experiments was approximately 1.010. The solution is also allowed to stand for some time to attain the room temperature. It is then pumped to the overhead reservoir tank from where it is very slowly transferred to the basin through the finely perforated "lip". The rate at which the salt solution enters the basin is regulated with a valve along the piping system from the reservoir to the basin. The salt water being "heavier" than the fresh water, it stays below, displacing the fresh water upwards. The flow is turned off when the desired total height is reached.

The practical density profile of the water in the basin is obtained by using the probe and the digital multimeter to find the resistance at intervals of two inches from the top to the bottom of the basin. With the appropriate calibration curve the densities at the various points are known. Figure 8 is what a typical profiles look like. At the transition layer the interval at which resistance readings are taken is smaller (about 1/2 inch). To increase the accuracy of the measurements two probes differently calibrated are used. The stratification for a medium is $(\Delta\rho/\rho_o)$.

Penetration Experiment

For all the experiments the propeller depth (h_o) was about one propeller diameter. Trial runs are first made to determine the range of propeller revolutions per second (rps) that make the jet have good penetrations without hitting the floor of the basin. The critical

velocity that makes the jet get to the bottom may also be obtained approximately from the relationship $V_o^2/2g = (\Delta\rho/\rho_o)\Delta h_{to}$. The following steps were followed:

1. Start the propeller pump and adjust the rps until it is within the determined range but more to the low side.
2. Turn on the dye stuff so that it gets to the propeller and penetrates with the jet.
3. Read the propeller rps as well as the jet penetration depth. (the jet penetration depth is read from a vertical rule inside the basin and close to the propeller).
4. Shut off the power to the propeller and the dye flow.
5. Wait about ten minutes and then determine the density profile again.

The experiment is successful only if the later density profile approximates closely to the initial one because this would indicate that the experimental conditions did not change. Ideally a successful experiment takes less than one minute to complete to prevent mixing.

For each density profile penetration depths are obtained for different propeller rps.

CHAPTER IV

PENETRATION EXPERIMENTAL RESULTS

Data Reduction

The data obtained for each experiment are the propeller rps and the penetration depth while the other parameters like the stratification of the medium and the thermocline depth are known before the experiment. From the propeller calibration curve in a uniform medium (Figure 22) the propeller induced central velocity, V_o, is obtained for each rps.

For each geometry the non-dimensionalised difference between the penetration depth and the thermocline depth, h_{st} is plotted against one half of the square of the densimetric Froude number $V_o^2 / 2g(\Delta\rho/\rho_o)\Delta h_{to}$, Figure 9.

Deductions

From the plots the following deductions were made:

1. The densimetric Froude number is approximately constant for any one geometry for varying values of V_o.
2. Short jets appear to achieve less penetration and have higher Fr_d.

In the light of jet penetration depth analysis (Appendix C), and in the absence of other overriding factors, the plots of h_{st} versus $1/2(Fr_d)^2$ should be exponential curves and Fr_d should change with V_o.

More importantly short jets should achieve more penetration rather than less and a lower rather than higher Fr_d. A possible explanation of the descrepancies may be that some other factors that have larger effects are present. These factors render the calibration of V_o in the proximity of a thermocline invalid and that V_o is actually reduced the more the thermocline is closer to the propeller.

Plots of one half of the square of another version of the densimetric Froude number, $V_o^2 / 2g(\Delta\rho/\rho_o)\Delta h_{st}$ against the non-dimensional difference between the thermocline depth and the propeller depth, Δh^*_{to} for different geometries also had the same features as above.

As a consequence of the results obtained above it became necessary to investigate how the propeller flow rate varies with the distance of the thermocline from the propeller and compare the results with what was obtained from flow studies in a uniform medium.

Flow Measurements

This chapter presents the procedures employed to set an effective method for measuring the propeller flow rate (Q_p) that will give about the same result as that obtained by the flow visualization method.

Method and Procedure

The concept that total pressure is the sum of static pressure and velocity pressure was employed to make direct velocity measurements at points along the propeller jet. Using the volume flow analysis (Appendix D) the jet flow rates at the points were obtained.

The basic apparatus used for the experiment was a "U" tube manometer. In a typical experiment everything is set up as in the pene-

tration experiment except that the basin is filled with only fresh water. The manometer is screwed vertically to the side of the tank and polystyrene extension tubes are connected to the manometer legs. One leg of the extension tube is held through a clamp to a point directly below the centerline of the propeller. The other leg is held at a point in the basin very remote from the propeller but of the same vertical height.

This sequence is followed in performing an experiment.

1. Check for air bubbles along the lines. If present blow or suck through until they are expelled.
2. Note the levels of water in the manometer legs by using the scale.
3. Run the propeller at a speed high enough to produce an easily readable difference in the water levels in the manometer but not enough to introduce air bubbles in the basin.
4. Read the propeller speed and the manometric water levels.
5. Keeping every other thing constant, move the manometer extension pipe under the propeller (1/2 inch at a time) along the propeller diameter and take manometric height readings at each point.
6. Continue taking readings until there is no noticeable change in the manometer readings.
7. Repeat the process with the manometer legs at different vertical height below the propeller.

Data Reduction

Plots of the pressure profiles for different vertical distances

below the propeller are shown in Figure 11. With the volume flow analysis of Appendix D, the average velocity of the propeller was calculated for each vertical height used in the experiment. The various values obtained were compared with that obtained by the visualization method for the same speed.

The values obtained from the test at 4 1/2 inches below the propeller gave the best comparative results. Hence 4 1/2 inches below the propeller was chosen as a representative point at which velocity pressure readings could be taken.

CHAPTER V

PROPELLER RE-CALIBRATION

The first step in the re-calibration of the propeller in the proximity of a downstream obstruction was to study the variation of the flow rate with the distance of the obstruction from the propeller.

Flow Rate Variation

The method employed in the study of flow rate variation was basically the flow measurement method of the previous chapter. The point of measurement was 4 1/2 inches below the propeller. For the obstruction a flat plate was used. With the plate at different distances from the propeller and the propeller running at the same speed, pressure readings were taken and then converted to volume flow rates.

The ratio of the flow rate so obtained Q_a and that obtained in an unobstructed flow Q_i, was plotted against the non-dimensionalized distance of the propeller to the plate, L_o*. This is shown in Figure 12. The curve shows that as the plate (obstruction) is brought closer to the propeller the flow rate decreases as compared to the flow rate in an unobstructed flow. The curve becomes asymptotic as the plate distance to the propeller increases tending to:

$$\frac{\text{Obstructed flow rate}}{\text{Unobstructed flow rate}} = \frac{Q_a}{Q_i} = 1$$

Since it is apparent that when the plate is at the propeller posi-

tion there will be no net down flow, the curve was produced backwards to the origin.

Correction Curve

Experiments showed that the curve was independent of the propeller speed as long as the speed was high enough to cause the jet to get to the plate. Hence for a solid obstruction the curve could be used as a correction curve. When the obstruction is the stratification of the medium, the flow rate variation with the position of the thermocline may be dependent on the propeller speed.

Re-calibration Procedure

Definitions:

h_o = Propeller depth

h_t = Thermocline depth

h_s = Depth of stagnation point

L_o = Distance from propeller to plate

L_1 = Distance from propeller to thermocline $(h_t - h_o)$, h_{to}

L_2 = Distance from stagnation point to propeller $(h_s - h_o)$, h_{so}

V_o = Propeller velocity calibrated in uniform medium

V_c = "Corrected" propeller velocity

The length parameters are made non-dimensional by dividing by the propeller diameter and as usual they are asterisked.

In re-calibrating the propeller for flow in the presence of a downstream obstruction, the objective is to find a relationship between L_o^*, L_1^*, and L_2^* that makes the curve of Δh_{so}^* against $V_c^2 / 2g(\Delta\rho / \rho_o)$ Δh_{so}, (Figure 13) for the different geometries (different L_1^*)

collapse.

The "corrected" propeller velocity V_c is obtained by multiplying V_o by C_1, a correction factor. For any value of L_o^*, the corresponding value of Q_a/Q_i from the correction curve gives the correction factor. V_c is substituted for V_o in the plot of Figure 13. By a trial and error process a relationship $L_o^* = (aL_1^* + bL_2^*)/(a + b)$ that makes the curves collapse is sought (a and b are positive constants). Some of the curves obtained with different values of a and b are shown in Figures 14 - 16. The relationship that nearly collapsed the curves was $L_o^* = L_1^*$, that is a = 1 and b = 0, for the short jets investigated.

CHAPTER VI

RESULTS AND DISCUSSION

Penetration Depth

The central velocity at any point h, along the propeller jet V(h), derived in Appendix C is

$$V(h) = V_o \exp(-Kh/D_p) - \left(2g \int_{h_t}^{h_s} (\Delta\rho/\rho_o)\, dh\right)^{1/2} \qquad \text{C-10b}$$

(All the terms have their usual meanings.)

The exponential term (it could be quadratic also) represents the jet decay due to viscous dissipation while the integral term is the effect of stratification.

At stagnation point the velocity is zero:

$$V(h_s) = 0$$

and if h_s, D_p and V_o are known K can be found. Equation C-10b reduces to:

$$\frac{V_o^2}{2g} \exp(-Kh_s/D_p) = \left(\frac{\Delta\rho}{\rho_o}\right) h_{st} \qquad \text{C-10b}$$

Figure 11 shows the plot of Δh_{st}^* Vs $V_o^2 / 2g(\Delta\rho/\rho_o)\Delta h_{to}$. The plot, contrary to equation C-10b, indicates that jets which start off closer to the thermocline achieve less penetration for the same propeller velocity. This suggests that the propeller velocity, V_o, is actually reduced when the thermocline is close to the propeller. Hence any propeller calibration made in an unstratified medium may not be correctly applied in a stratified medium. The jet penetration depth

for any given propeller velocity is dependent on the position of the thermocline.

Givens (12) presents data that relate the normalized penetration depth Z_p^*, to the normalized thermocline location, Z_T^*, of the same model of propeller pump jet for various values of R_i. His data shows that as Z_T^* increases (i.e., the metalimnion is close to the surface), Z_p^* increases for a constant R_i (Figure 17). This is in line with the findings of the present study. Sources of errors are very common in this type of experiments and reproducing experiments is difficult. Here are some of the sources.

The magnetic pick-up does not produce adequate signals at low r.p.m. while the hasler tachometer because of its weight on the propeller shaft reduces the r.p.m. The coating on the conductivity probe is constantly being eroded by the salt solution and it quickly produces readings different from those used for its calibration even for the same salt water conditions. The initial and final density profiles in any experiment are never exactly the same which means that experimental conditions are really not constant.

As an attempt to reduce the errors and uncertainties in the experiments, four undergraduate Mechanical Engineering Seniors at Oklahoma State University under the supervision of Dr. D. K. McLaughlin tried different alternative techniques of carrying out the experiments. The students were M. A. Haywood, T. F. Maloney, B. E. McKillop and G. F. Sander. Their findings indicate that especially for large propeller-thermocline distances, the viscous dissipation effects can be greater than the propeller calibration errors and that jet penetration decreases as the propeller-thermocline distance is increased

beyond about two propeller diameters. For a propeller-thermocline distance less than two propeller diameters their results agree with this study that the calibration errors are greater than those of viscous dissipation. Close examination of their graph of jet penetration against thermocline distance figure 18 shows that the curve has a positive gradient trend for thermocline distance of less than about two and a negative gradient for thermocline distance above two.

However in the analysis of their results, they had used the theoritical thermocline position as the actual position. Naturally and even in the laboratory also (using salt water and fresh water), a clear cut thermocline line is not attained. The thermocline is normally a transition layer which varies in thickness. A better approximation of the thermocline position is about half way through the layer. Experiments show that the mean thermocline position moves up relative to the theoretical value and that the upward movement increases as the salt water (hypolimnium) thickness decreases. With this background the agreement in trend between their experiments and this study becomes more obvious. Their result for thermocline position of three diameters may have been influenced by the nearness of the basin floor. Their findings suggest that for a wide range of thermocline positions, the over all relationship between the jet penetration and the propeller-thermocline separation may be more complex than analyses suggest. A summary of their experiment is shown in Appendix E.

Attempts were made to perform the flow rate variation study with stratification instead of the plate as the obstruction, but this turned out to be an almost impossible experiment. It was not possible to

take all the readings that count, with the propeller speed being kept constant without appreciable mixing of the basin, which render the test invalid.

Propeller Re-Calibration

As stated earlier, the relationship:

$$L_o^* = (aL_1^* + bL_2^*)/(a + b)$$

that makes the curves of h_{so}^* Vs $V_c^2/2g(\Delta\rho/\rho_o)\Delta h_{so}$ collapse gives the clue as to how the experiments with the plate as the obstruction can be applied to the situation where the thermocline is the "obstruction".

The data represented in figures 14-16 show that the curves get more apart when b is greater than a and that they come closer when a is greater than b. The extent of the divergence or convergence increase with the absolute difference between a and b.

The significance of the fact that the relationship that brought the curves closest to collapsing was:

$$L_o^* = L_1^*$$

is that the thermocline has almost the same effect as the flat plate, for the range of parameters of the experiments. The fact that the correction curve may vary with the propeller speed may be a contributing factor to the curves not collapsing completely. However this is not apparent from the results. The failure of the curves to completely collapse may be due partly to those sources of error.

CHAPTER VII

CONCLUSIONS

Summary

The flow field induced by a model of the axial-flow propeller pump for destratifying lakes was studied, initially to find how the penetration depth is related to the metalimnion depth. The result was contrary to what was expected. When the propeller is very close to the metalimnion the jets achieve less penetration than when the thermocline is further away for the same densimetric Froude number, Fr_d. This result meant that the calibration of the propeller which states that that flow rate is a linear function of the propeller speed is not true if the thermocline is very close to the propeller. The propeller should be re-calibrated to accomodate this finding. The data from this study presents the re-calibration procedures. A flat plate put in the place of the thermocline has similar effects as the thermocline. That was the fact that made it possible to apply the results obtained using the plate to the situation of the thermocline.

Conclusions

The main conclusions from this study are:

1. In the study of the flow field of a propeller pump jet in a stratified medium the principal parameter is one half of the square

of the densimetric Froude number, $V^2 / 2g\Delta\rho/\rho_o h$.

2. Propeller performance (V_o) is reduced by a downstream obstruction.
3. V_o is also reduced when the thermocline is very high making very short jets achieve less, rather than more penetration.
4. The curve of Q_a/Q_i versus L_o* (correction curve) is independent of the propeller speed, for a solid flat obstruction.
5. The thermocline has a similar effect as the flat plate on propeller performance, at least at very close spacings. In some cases, the distance to the mean location of the thermocline is the equivalent plate obstruction.
6. The curve of Q_a/Q_i versus L_o* obtained for a flat plate can be applied to a stratified flow field to "correct" the velocity of the propeller from its uniform medium "calibration", for the close proximity of a severe stratification.

Recommendation for Further Study

1. Penetration depth experiments in stratified media should be carried out over wide ranges of parameters and by a variety of methods.
2. The flow rate variation in stratified media with respect to the propeller speed should be further studied.

A SELECTED BIBLIOGRAPHY

(1) Abraham G., and W. D Eysink. "Jets Issuing Into Fluids With a Density Gradient." Journal of Hydraulic Research, Vol 7, No. 2 (April 1969), pp. 145-175.

(2) Baines, W. D. "Entrainment by a Plume or Jet at a Density Interface." Journal of Fluid Mechanics, Vol. 68, (April, 1974), pp. 309-320.

(3) Baines, W. D. "Turbulent Buoyant Plumes." Heat Transfer and Buoyant Convention. Vol. 1. 1977. Washington, DC: Hemisphere Publishing Corporation, pp. 235-250.

(4) Baumeister, T. Standard Handbook for Mechanical Engineers. 8th edition. 1978. New York: McGraw-Hill.

(5) Brush, L. M., Jr., F. C. McMichael, and C. Y. Kuo. Artificial Mixing of Density-Stratified Fluids: A Laboratory Investigation. Trenton: Water Resources Research Institute, Research Project B-005-NJ, 1968.

(6) Busnaina, A. A. "Numberical Simulation of Local Destratification of Lakes." (Unpublished M.S. Thesis, Oklahoma State University, 1979).

(7) Dake, J. M. K. and D. R. F. Harleman. "Thermal Stratification in Lakes: Analytical and Laboratory Studies." Water Resource Research, Vol. 5, No. 2 (April, 1969), pp. 485-495.

(8) Ditmars, J. D. Mixing of Density Stratified Impoundments with Buoyant Jets. Pasadena: W. M. Keck Laboratory of Hydraulics and Water Resources, California Institute of Technology, Report No. KH-R-22, 1970.

(9) Garton, J. E., and C. E. Rice. Improving the Quality of Water Releases from Reservoirs by Means of a Large Diameter Pump. Oklahoma City: Final Technical Report, OWRRI C-5228, Agreement No. 14-31-0001-4215, March 1976.

(10) Garton, J. E. and H. R. Jarrell. Demonstration of Water Quality Enhancement Through Use of the Garton Pump. Oklahoma City: Supplement to the Technical Completion Report, OWRRI C-5228-A, March 1976.

(11) Gibson, T. A. "Investigation of Artificial Lake Destratification - A Hydraulic Model Study." (Unpublished MS Thesis, Oklahoma State University, 1975).

(12) Givens, M. R. "Hydraulic Modeling of Local Destratification of Lakes Using Propeller Pumps." (Unpublished MS Thesis, Oklahoma State University, 1978).

(13) Kouba, G. E. "Modeling Inflows Into Stratified Lakes with Vertical Scale Distortion." (Unpublished MS Thesis, Oklahoma State University, 1974).

(14) Moon, J. J. "Enhancement of Release Water Quality by Localized Mixing - A Hydraulic Model Study." (Unpublished MS Thesis, Oklahoma State University, 1978).

(15) Moretti, P. M. "Investigation of Alternative Mixing Device for Lake by Model Studies." Technical Completion Report OWRRI A-050-Oklahoma. (Part I) Technical Completion Report. ER 76-ME-2. Stillwater: School of Mechanical and Aerospace Engineering, Oklahoma State University, July 1979.

(16) Moretti, P. M. and D. K. McLaughlin. "Hydraulic Modeling of Mixing of Stratified Lakes." Journal of the Hydraulic Division, ASCE, Vol. 103, No. HY 4 (April 1977), pp. 367-380.

(17) Punnett, R. R. "Destratification of Lake Arbuckle with a Cluster of Law-Energy Pumps." (Unpublished MS Thesis, Oklahoma State University, 1978).

(18) Quintero, J. E. "A Low Energy Lake Destratifier." (Unpublished Ph.D. dissertation, Oklahoma State University, 1973).

(19) Quintero, J. E. and J. E. Garton. "A Low Energy Lake Destratifier." Trans of ASAE, Vol. 16, No. 5 (1973), pp. 973-978.

(20) Schlichting, H. Boundary Layer Theory. 7th ed. New York: McGraw-Hill, 1979.

(21) Sharabianlou, N. "Hyraulic Modeling of Mechanical Destratification of Lakes." (Unpublished MS Thesis, Oklahoma State University, 1975).

(22) Strecker, R. G. "Design, Construction and Evaluation of Prototype Low-Energy Lake Destratifier." (Unpublished MS Thesis, Oklahoma State University, 1976).

(23) Strecker, R. G. et al. "Improving Lake Water Quality by Destratification." Trans. of ASAE, Vol. 20, No. 4 (1977), pp. 713-720.

(24) Symons, J. M. et al. "Impoundment Destratification for Raw Water Quality Control Using Mechanical or Diffused-Air-Pumping." Journal of American Water Works Association. Vol. 59, No. 10 (1967), pp. 1268-1281.

(25) Turner, J. S. "The Influence of Molecular Diffusivity on Turbulent Entrainment Across a Density Interface." Journal of Fluid Mechanics, Vol. 33 (1968), pp. 639-656.

(26) Vogel, S. J. "Similitude Investigation of Vertical Exaggeration in Stratified Lake Model." (Unpublished MS Thesis, Oklahoma State University, 1974).

APPENDIX A

TABLE AND FIGURES

TABLE I

COMPARISON OF MODELING PARAMETERS FOR DIFFERENT JET PENETRATION DEPTH EXPERIMENTS

Parameters	Experiment A	Experiment B	Experiment C
Maximum Depth, H	20 in	20 in	20 in
Density Stratification, $\Delta\rho/\rho_o$	0.01	0.01	0.01
Propeller Diameter, D_p	4.5 in	4.5 in	4.5 in
Non-dimensional Propeller to thermocline distance, h^*_{to}	1.9	1.4	1.0
Propeller Depth	3.5 in	3.5 in	3.5 in
Maximum Velocity	0.6 ft/sec	0.8 ft/sec	1.0 ft/sec

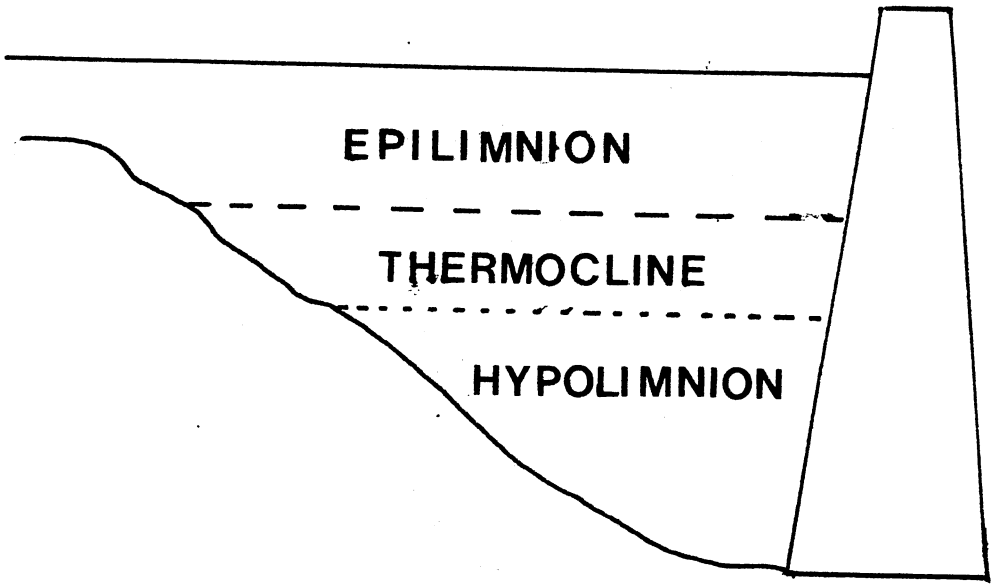

Figure 1. Typical Thermal Stratification Pattern

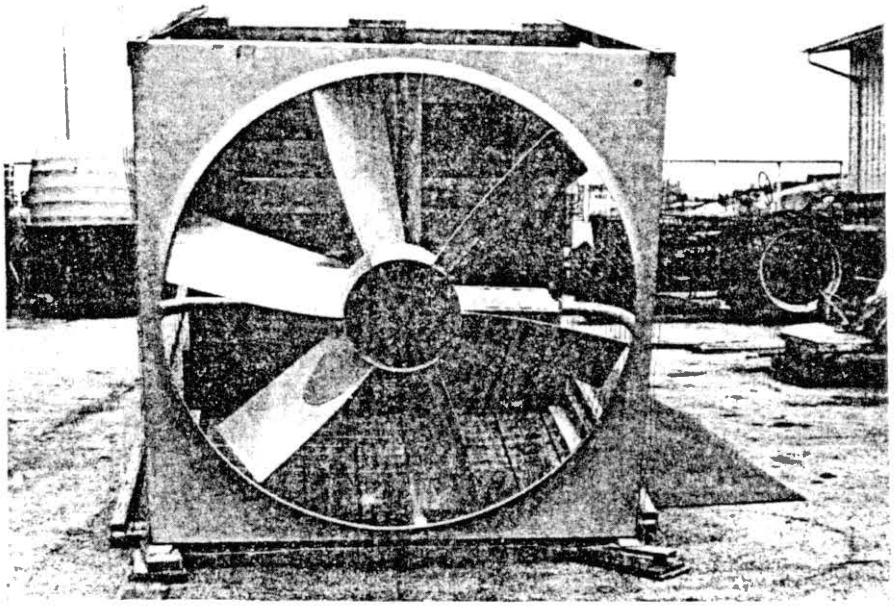

Figure 2. Photograph of the Garton Pump.

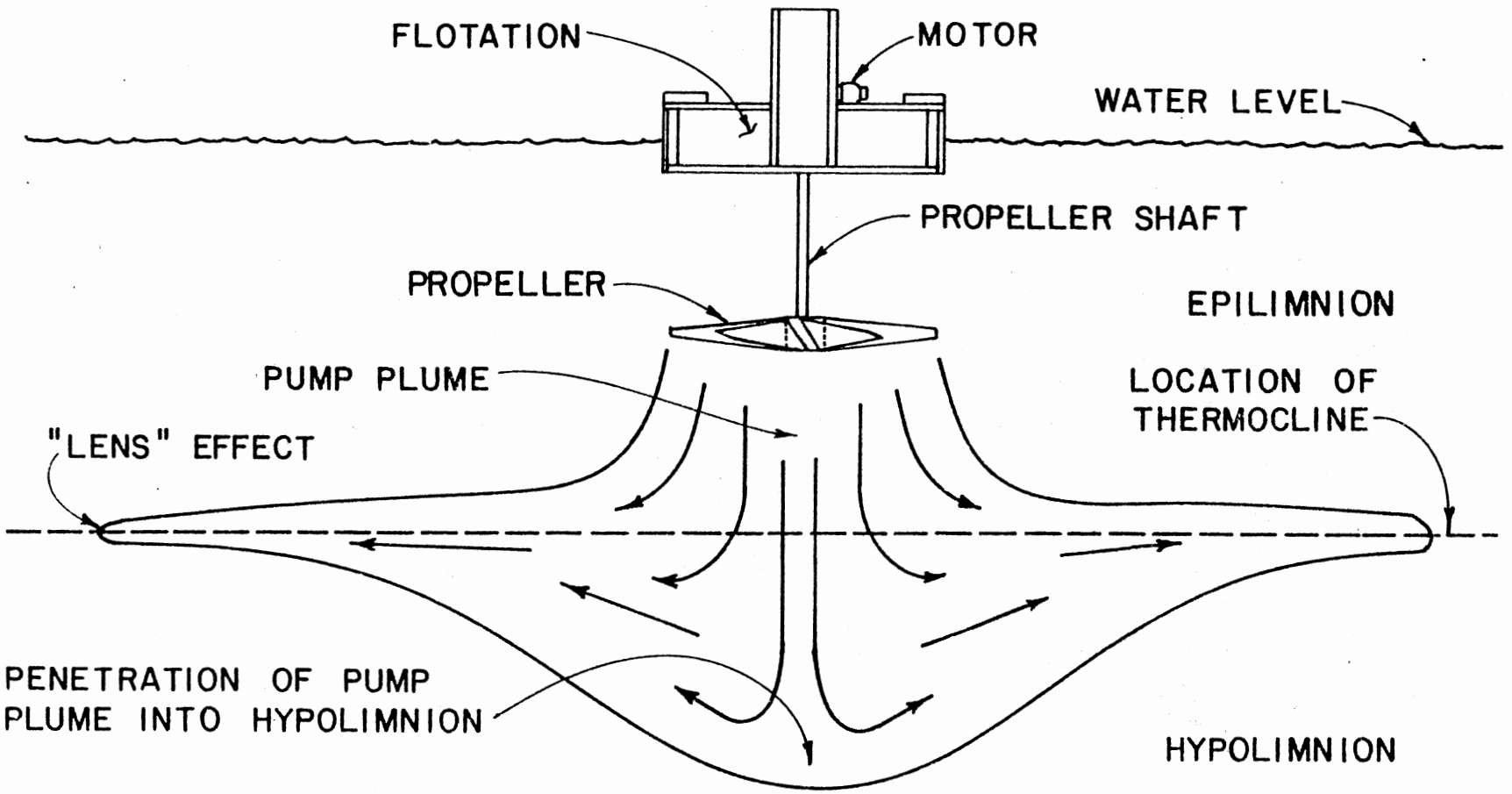

Figure 3. Schematic of a Typical Pump and its Flowfield.

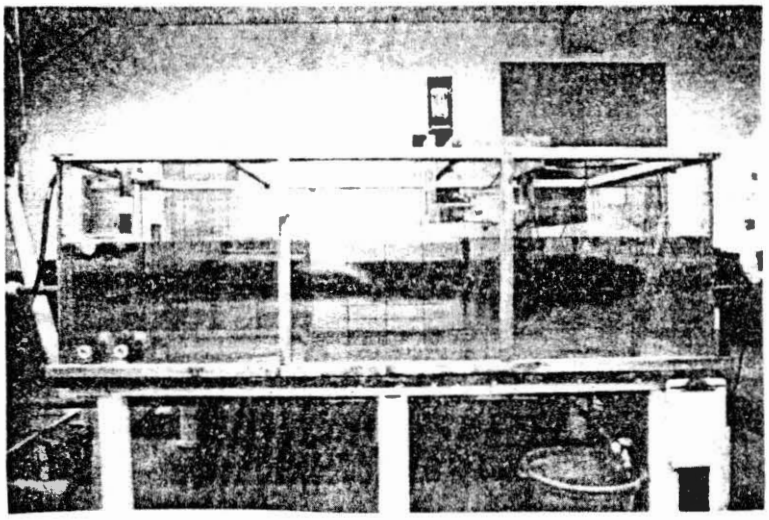

Figure 4. Photograph of the Test Basin

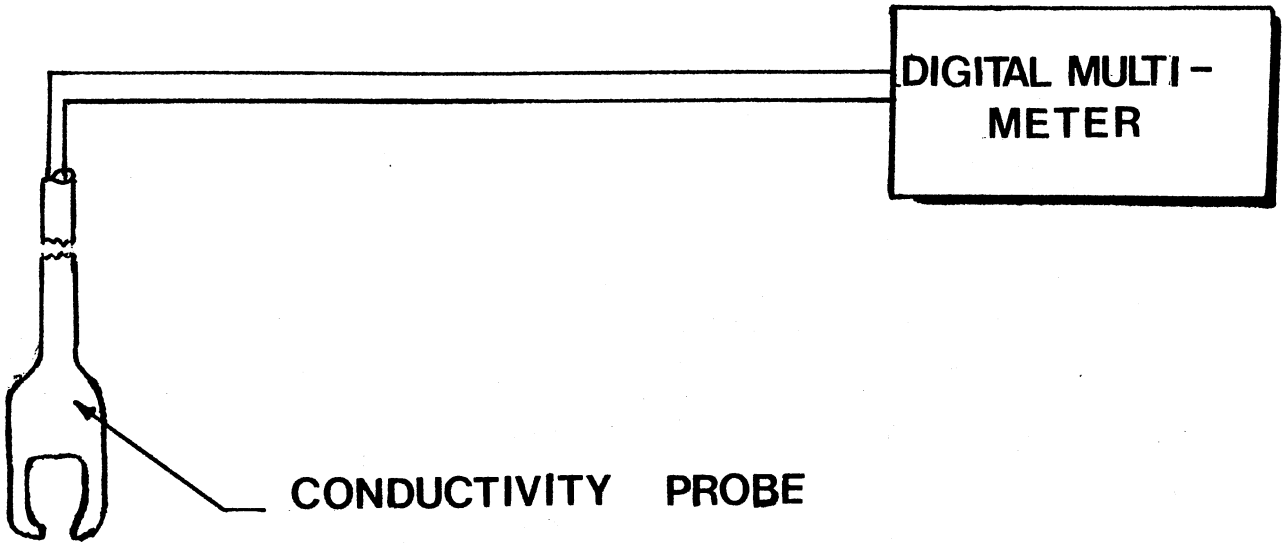

Figure 5. Schematic Drawing of Conductivity Unit

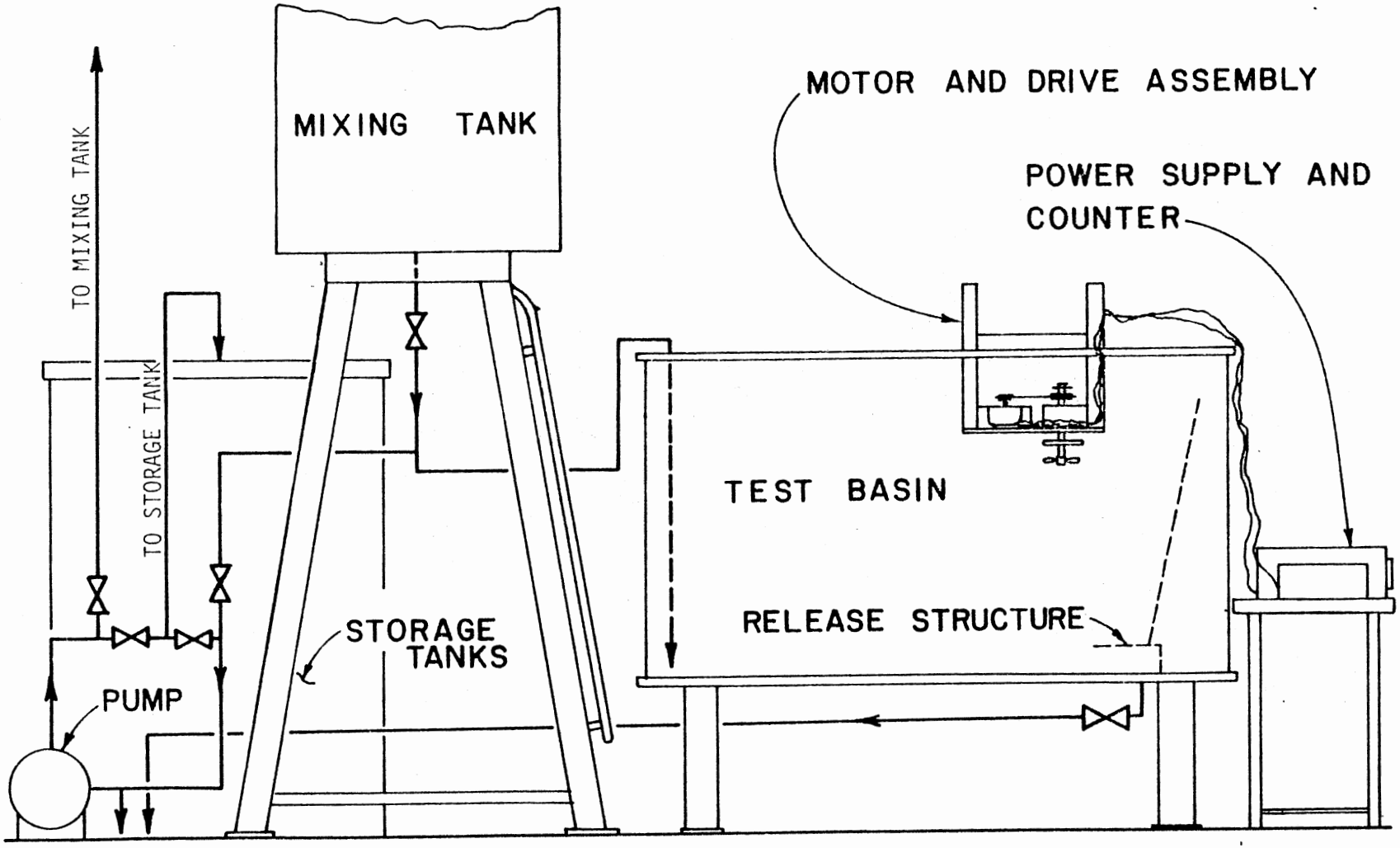

Figure 6. Schematic Drawing of Complete Laboratory Facility

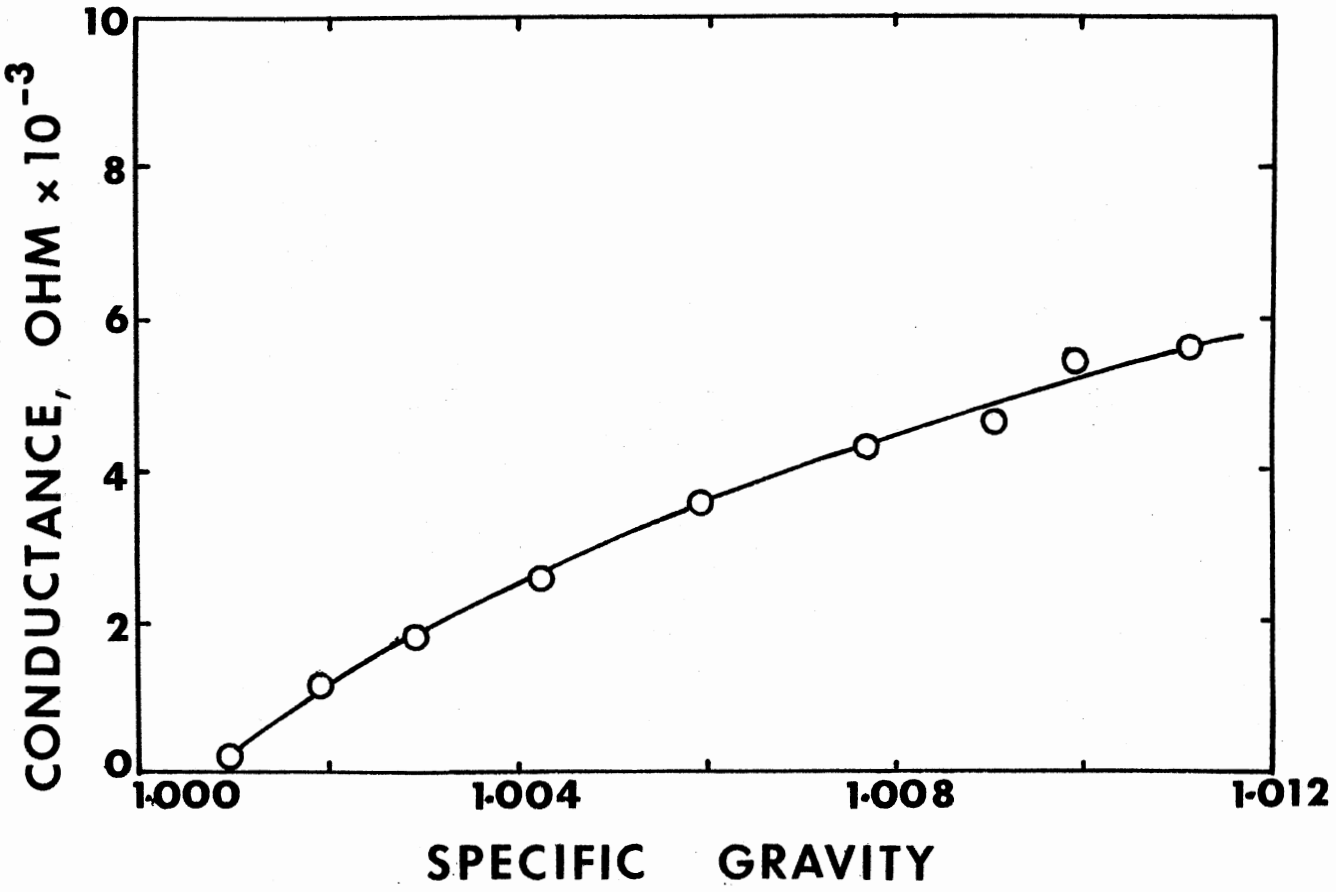

Figure 7. Sample Calibration Curve for Conductivity Probe

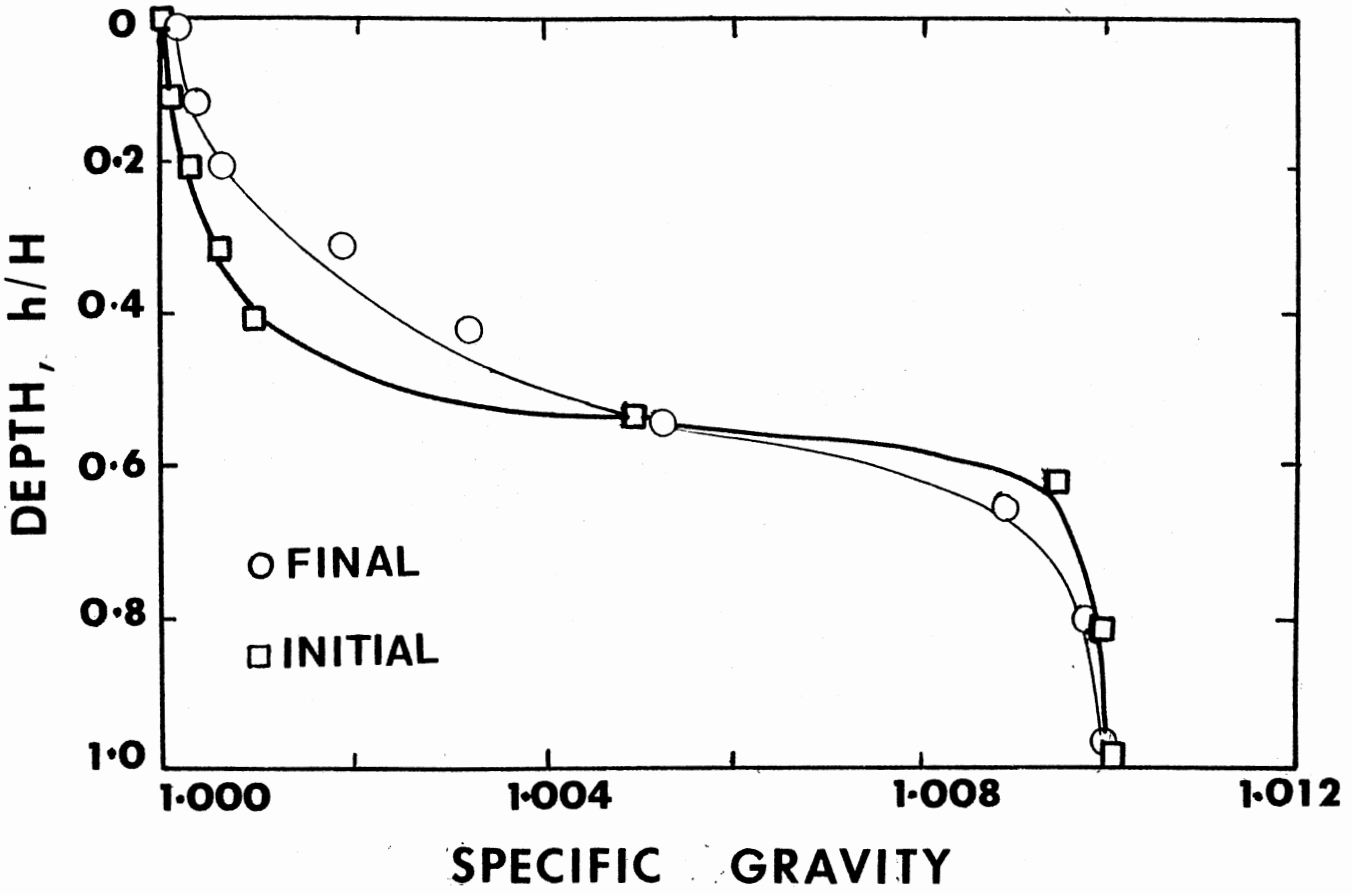

Figure 8. Initial and Final Density Profiles

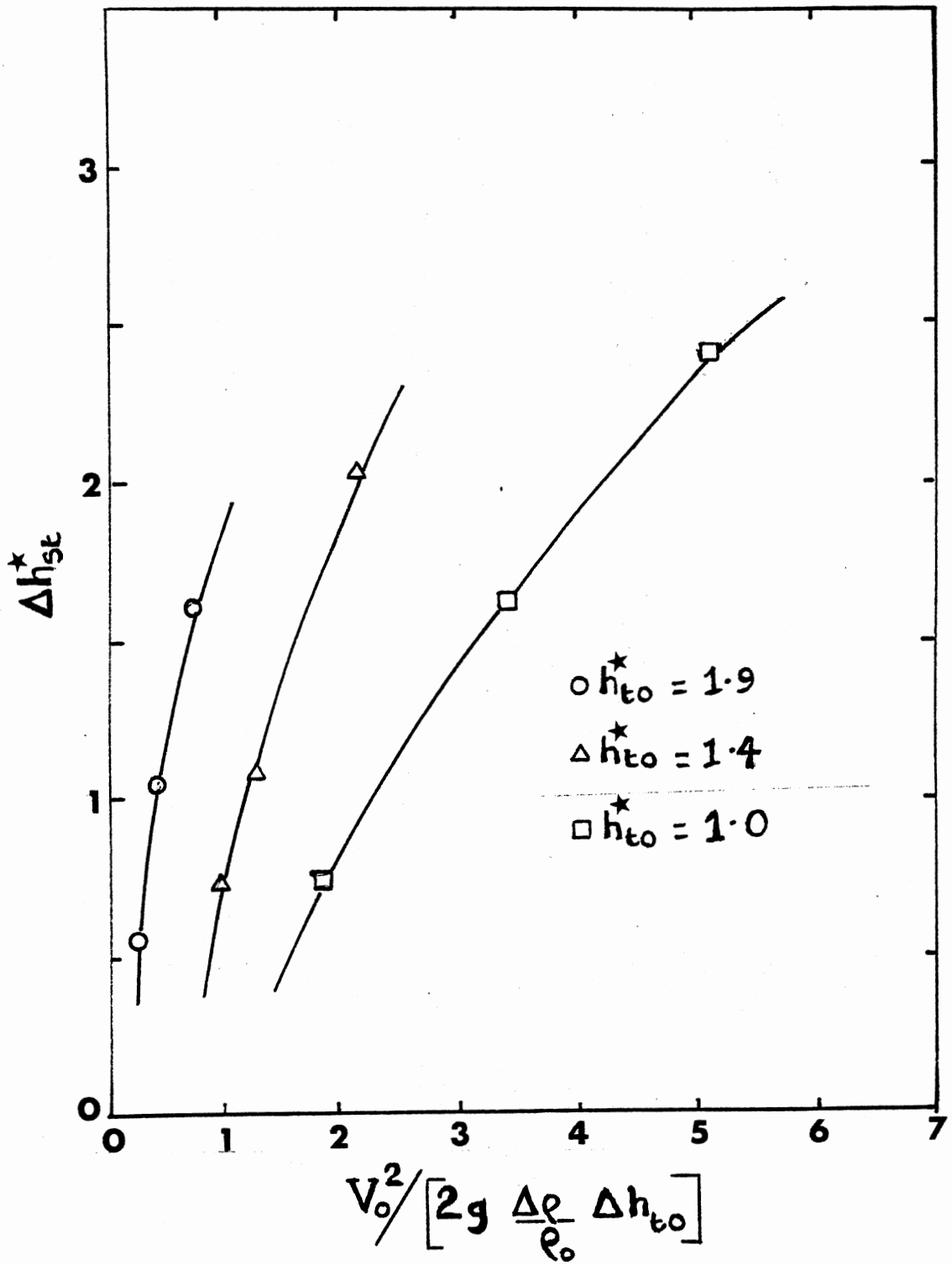

Figure 9. Non-dimensional Thermocline to Penetration Depth, Δh^*_{st} as a Function of One Half of the Square of the Densimetric Froude Number, $V_o^2 / 2g(\Delta\rho/\rho_o)\Delta h_{to}$

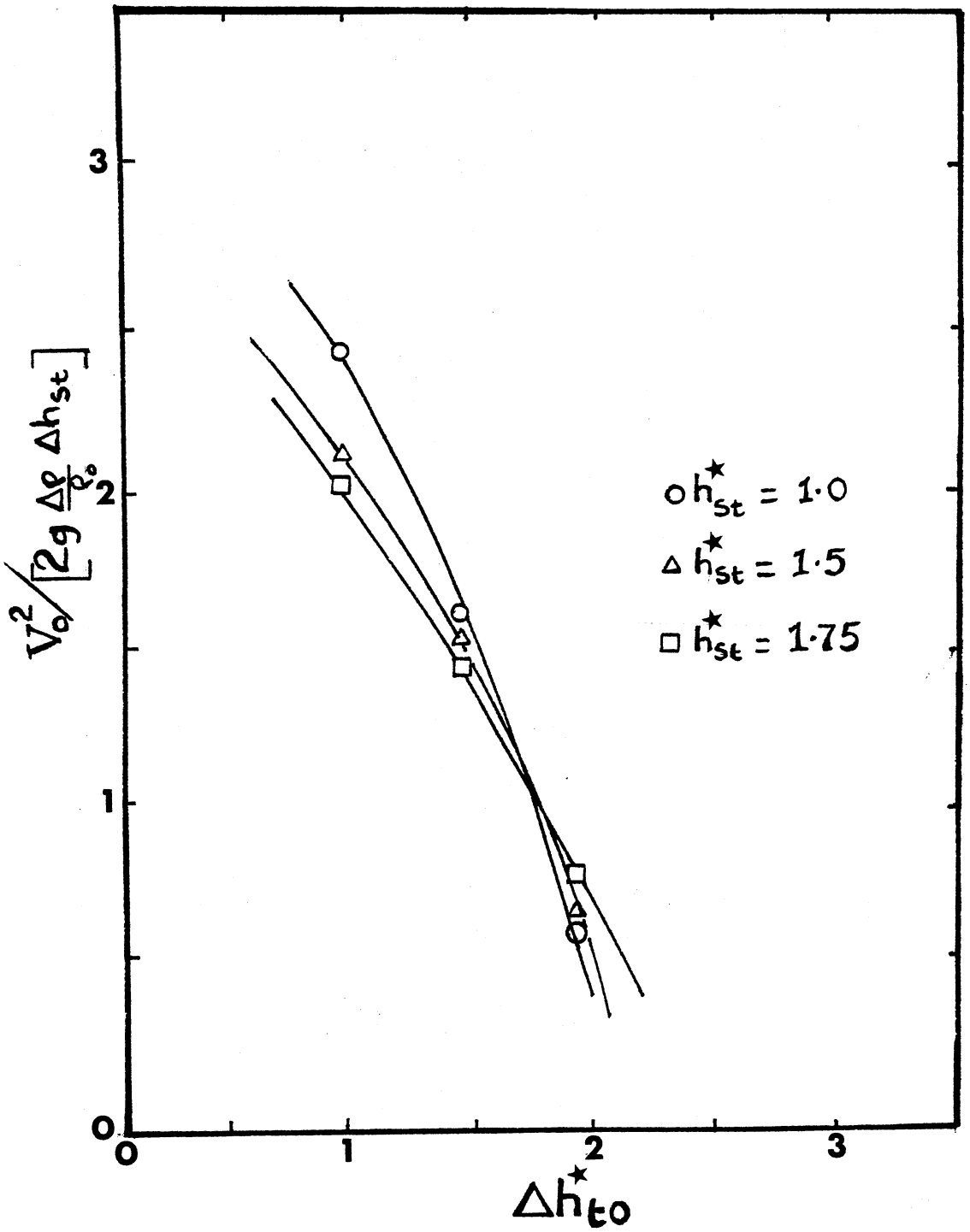

Figure 10. One Half the Square of the Densimetric Froude Number, $V_o^2 / 2g(\Delta\rho/\rho_o)\Delta h_{st}$ against the thermocline Depth Δh^*_{to}

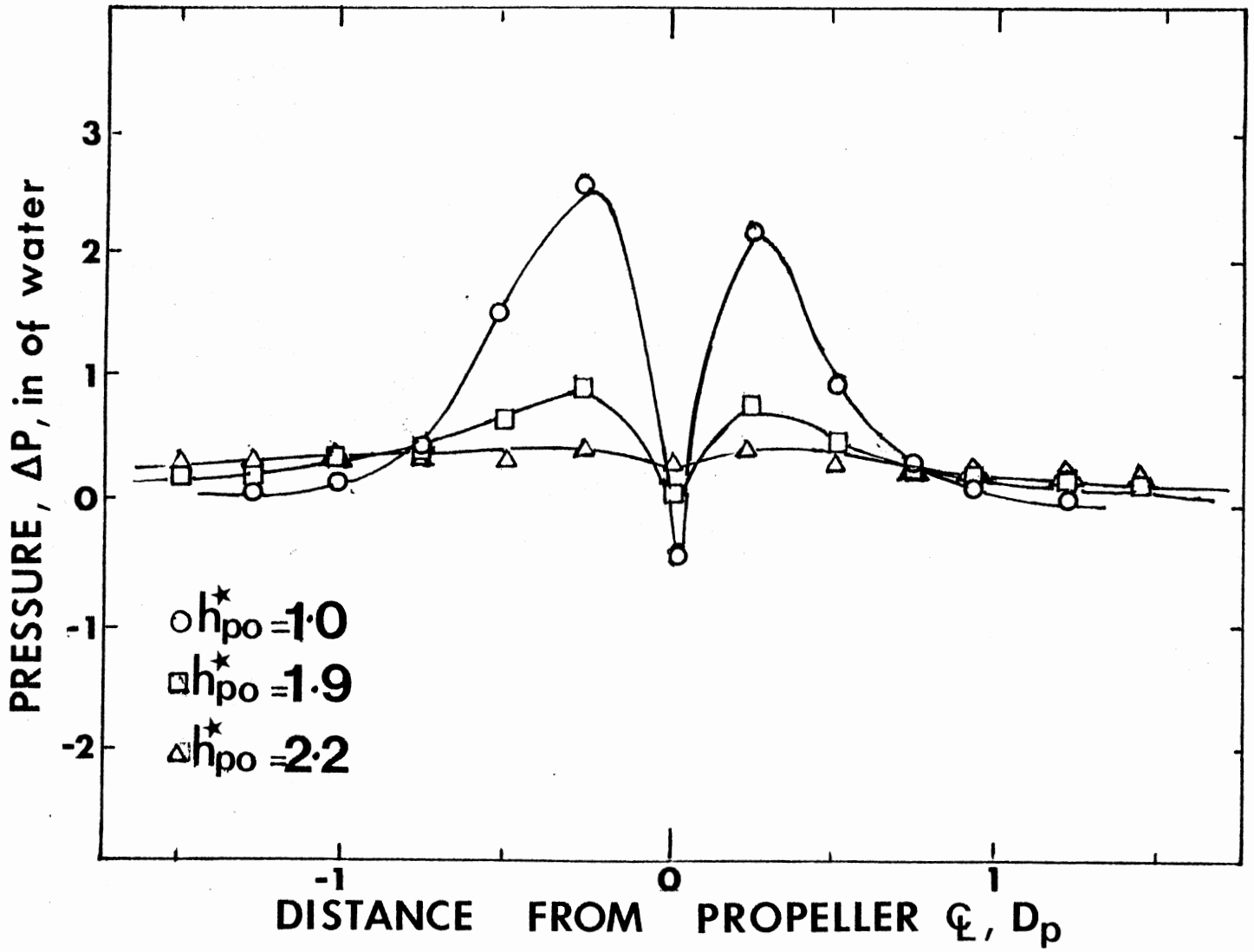

Figure 11. Pressure Profile as a Function of Distance from Propeller Center Line

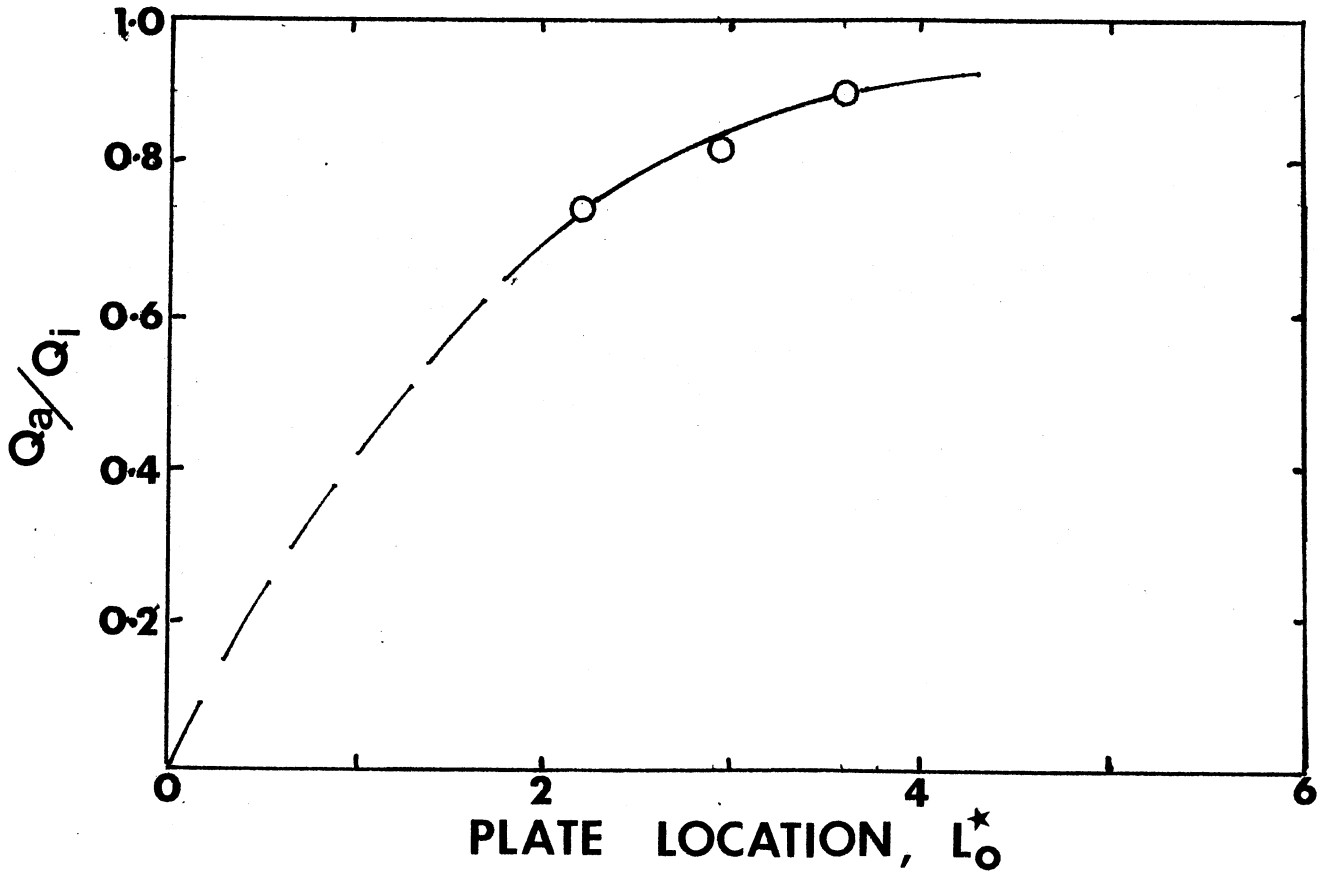

Figure 12. Normalized Flowrate, Q_a/Q_i, as a Function of Non-dimensionalized Flat Plate Location, L_o^*

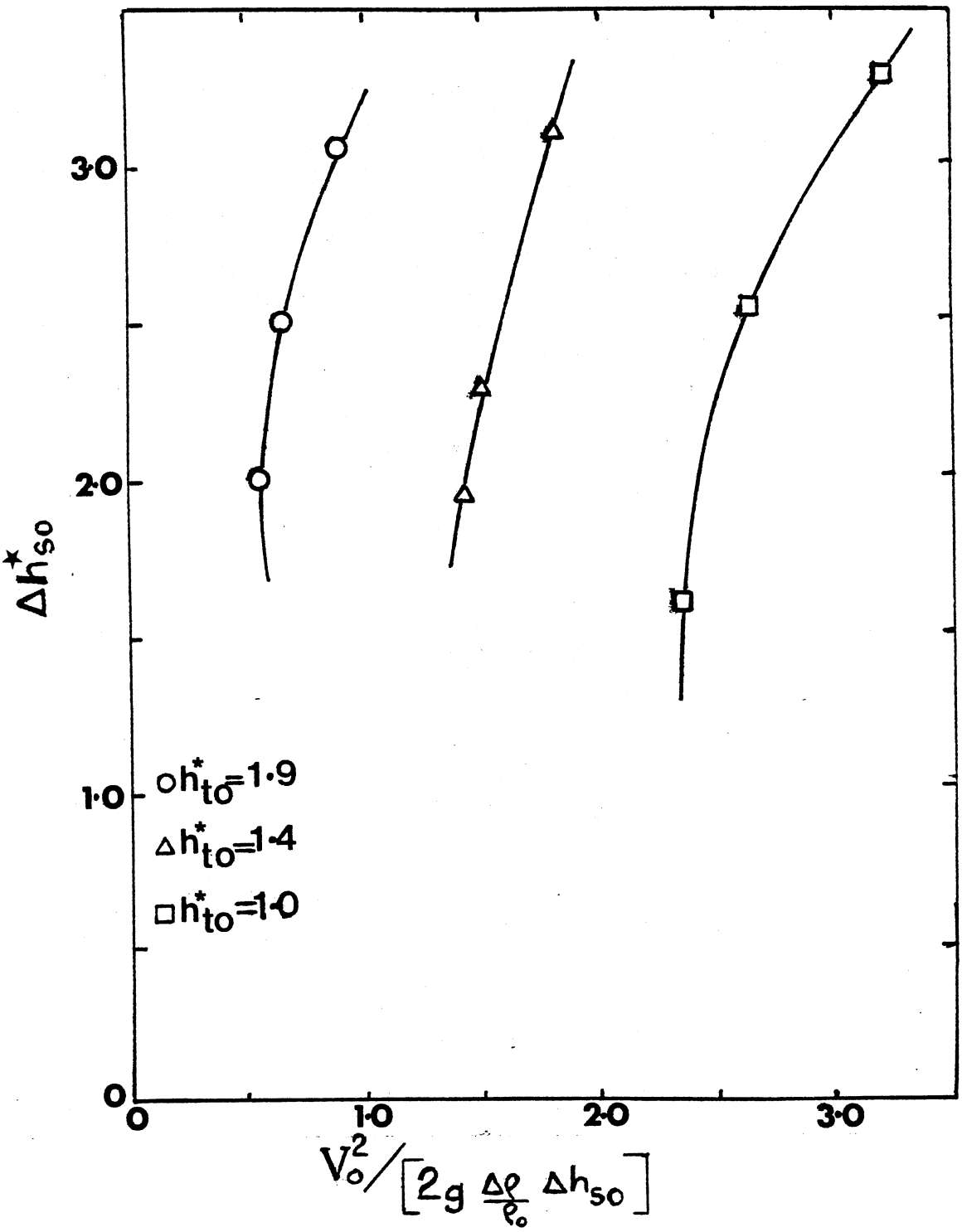

Figure 13. Non-dimensional Propeller to Penetration Depth, Δh^*_{so}, as a Function of One Half of the Square of Densimetric Froude Number, $V_o^2/\ 2g(\Delta\rho/\rho_o)\Delta h_{so}$

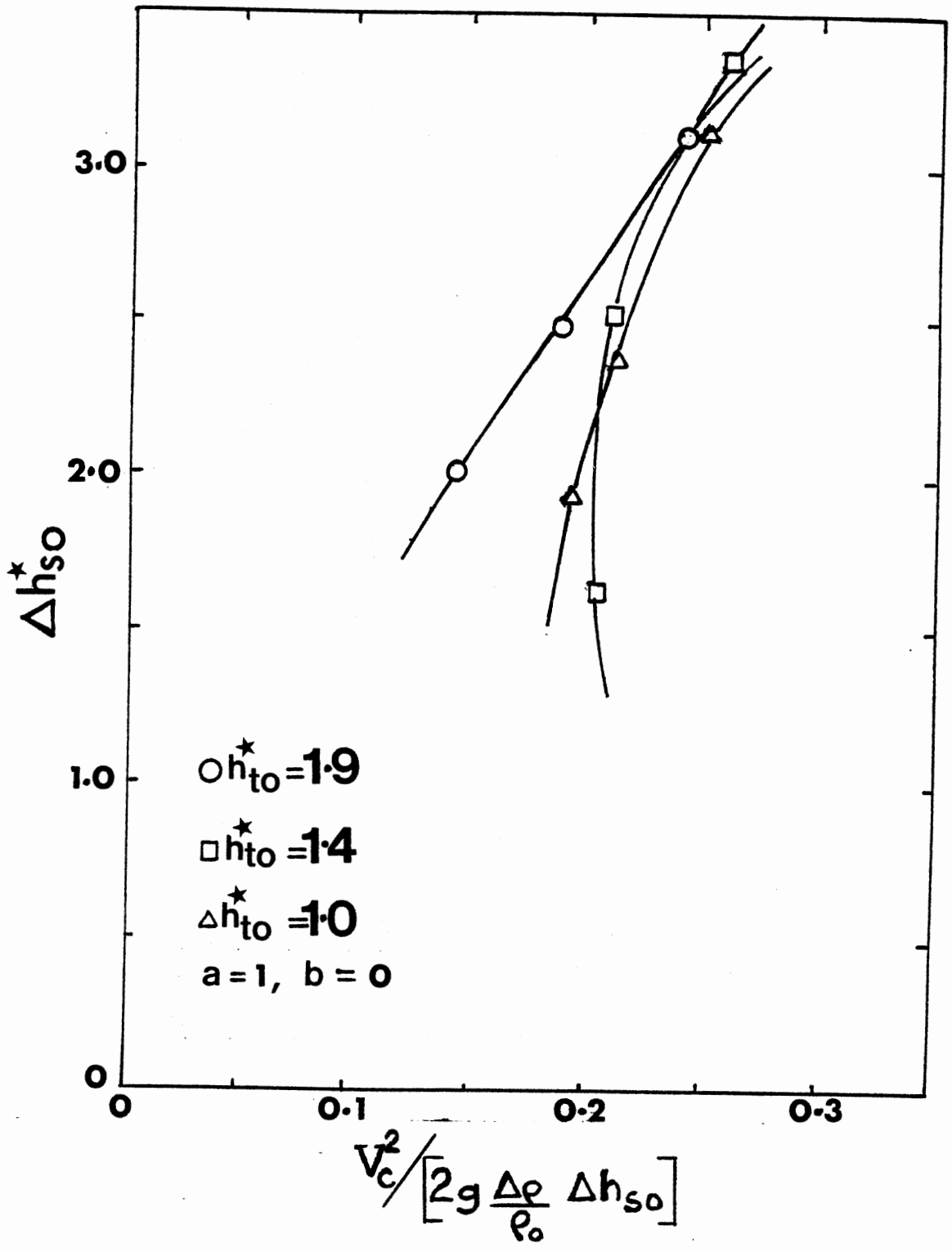

Figure 14. Non-dimensional Propeller to Penetration Depth, Δh^*_{so}, as a Function of One Half of the Square of Densimetric Froude Number, $V_c^2 / 2g(\Delta\rho/\rho_o)\Delta h_{so}$ (a=1, b=0)

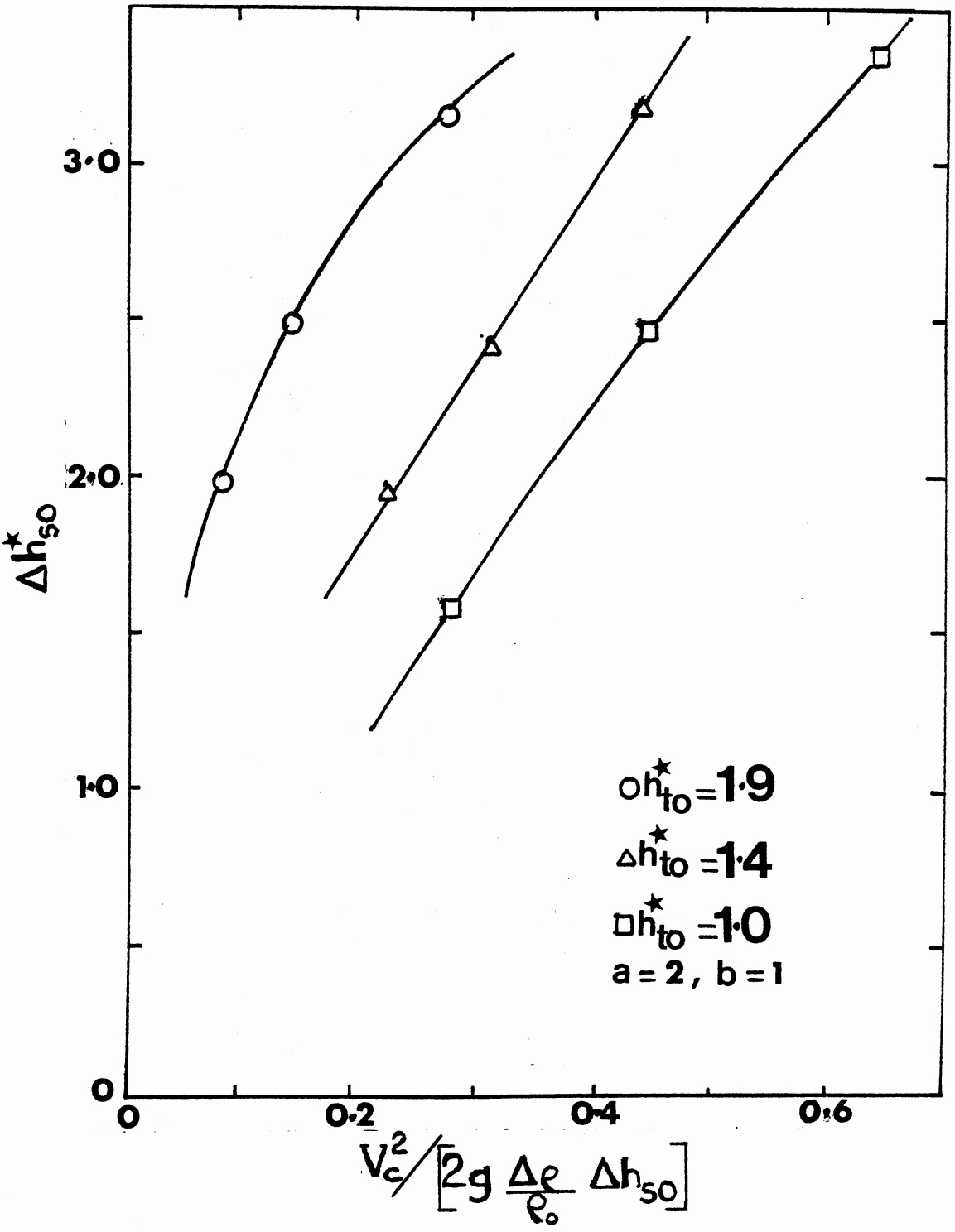

Figure 15. Non-dimensional Propeller to Penetration Depth, Δh^*_{so}, as a Function of One Half of the Square of Densimetric Froude Number, $V_c^2 / 2g(\Delta\rho/\rho_o)\Delta h_{so}$

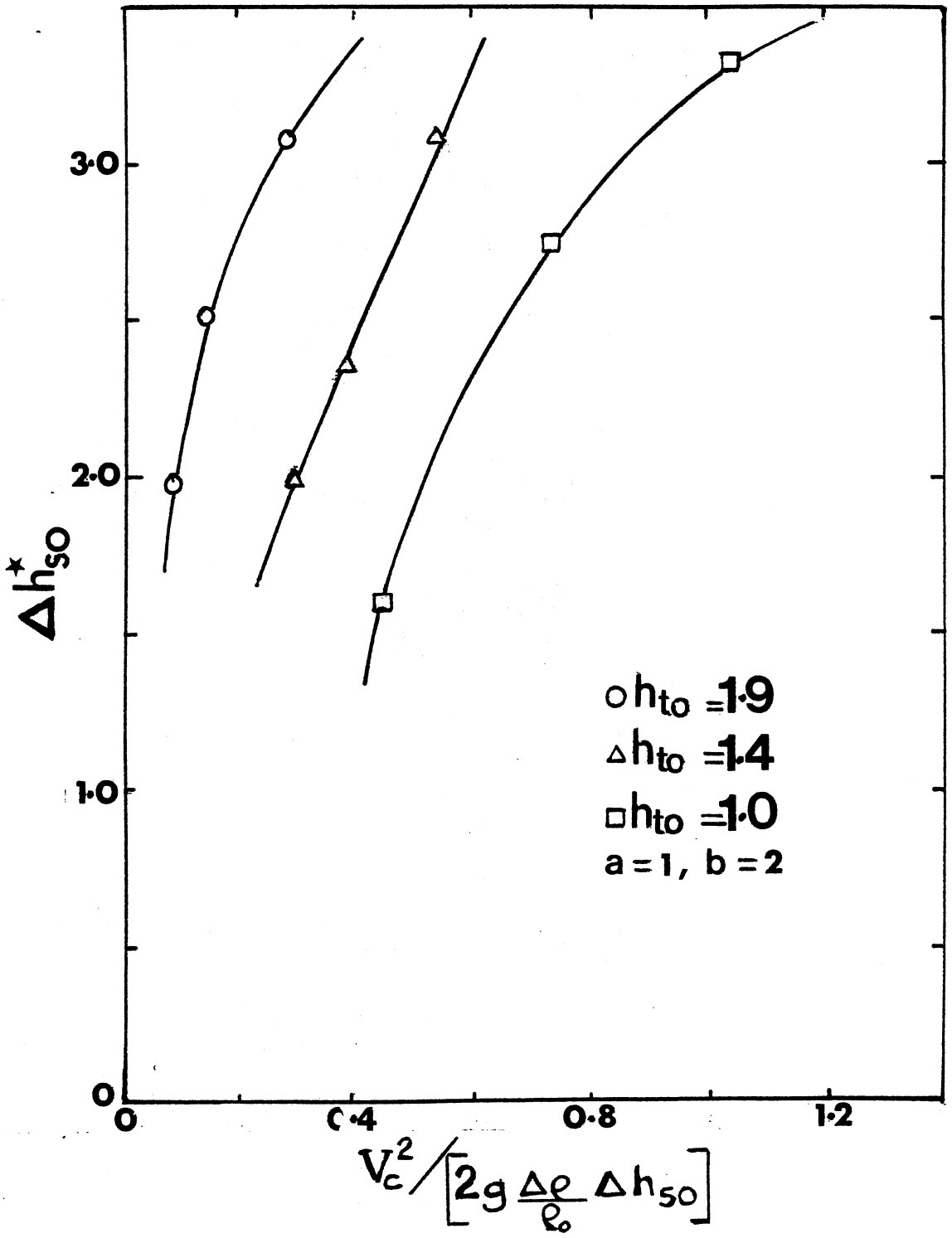

Figure 16. Non-dimensional Propeller to Penetration Depth, Δh^*_{so}, as a Function of One Half of the Square of Densimetric Froude Number, $V_c^2 / 2g(\Delta\rho/\rho_o)\Delta h_{so}$

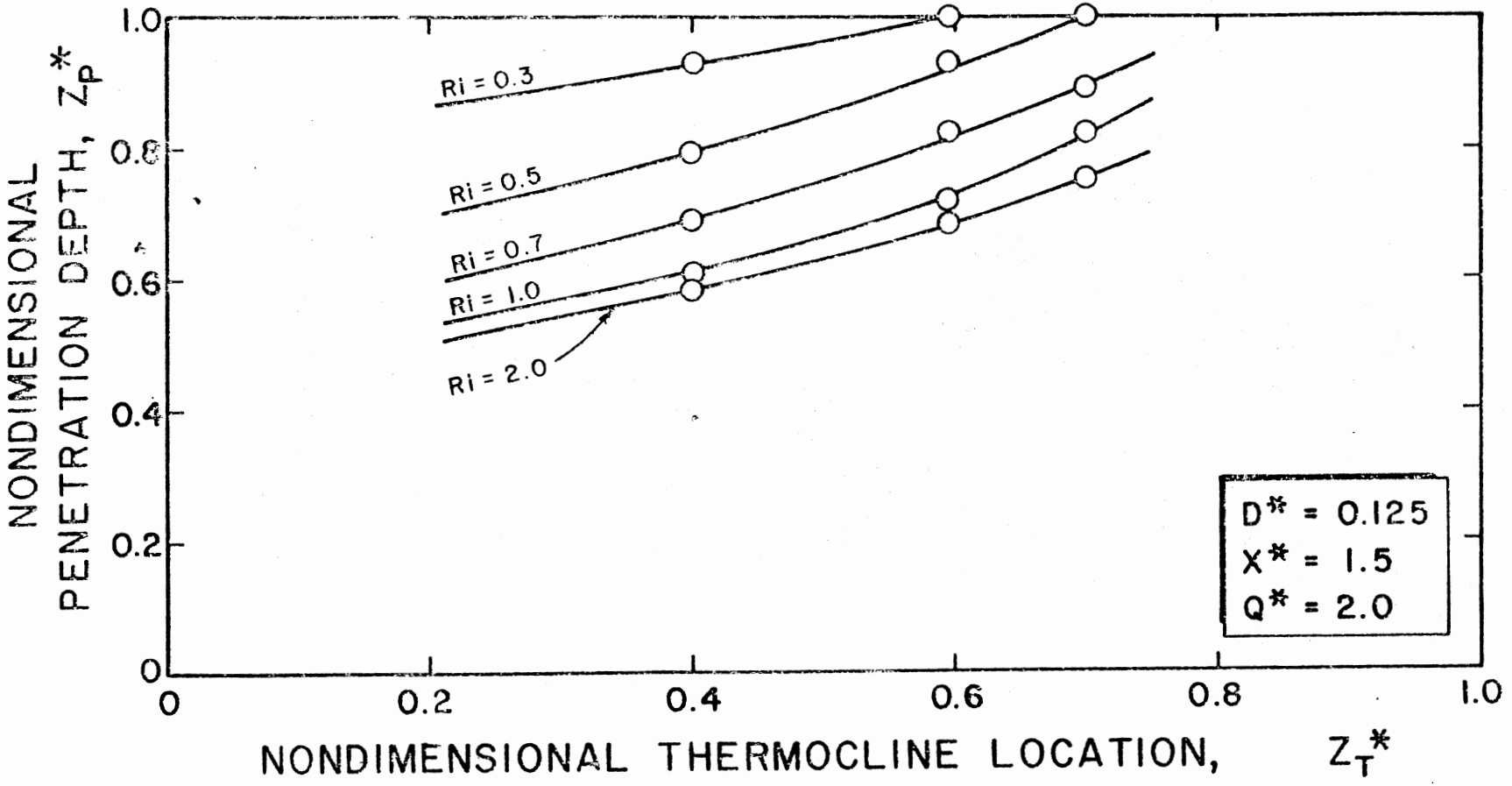

Figure 17. Effect of Thermocline Location on Penetration Depth [After Givens (12)]

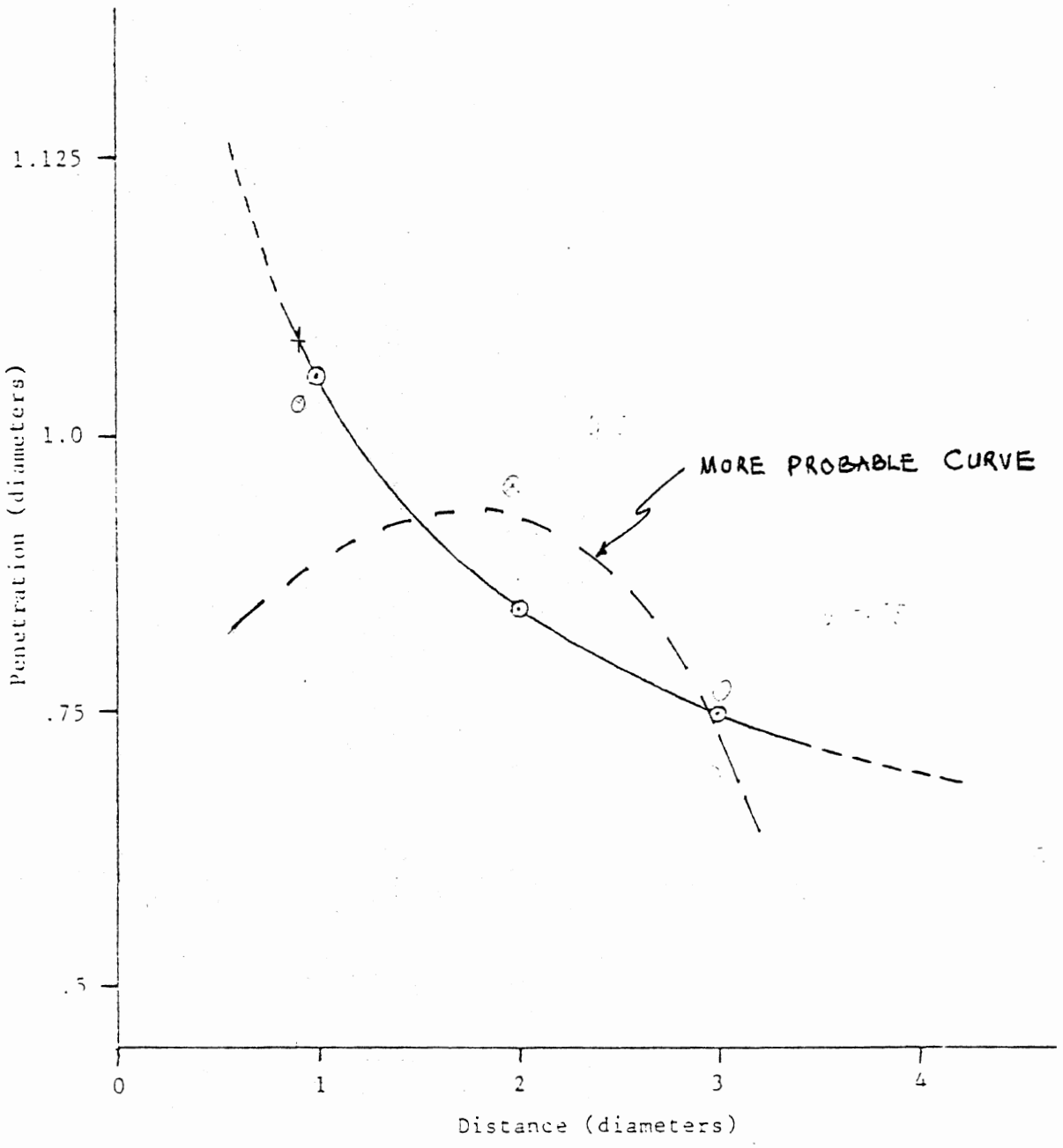

Figure 18. Jet Penetration as a Function of Separation of Propeller and Thermocline (Experiment of Haywood and Others)

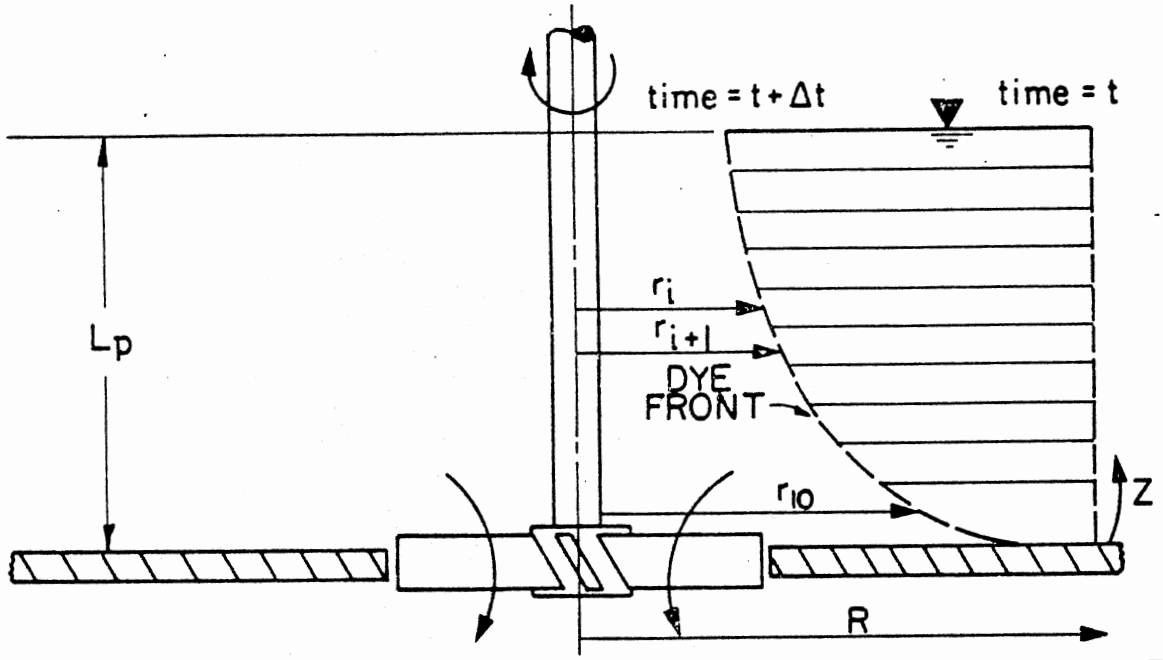

Figure 19. Drawing of the Flow Visualization [After Moon (14)]

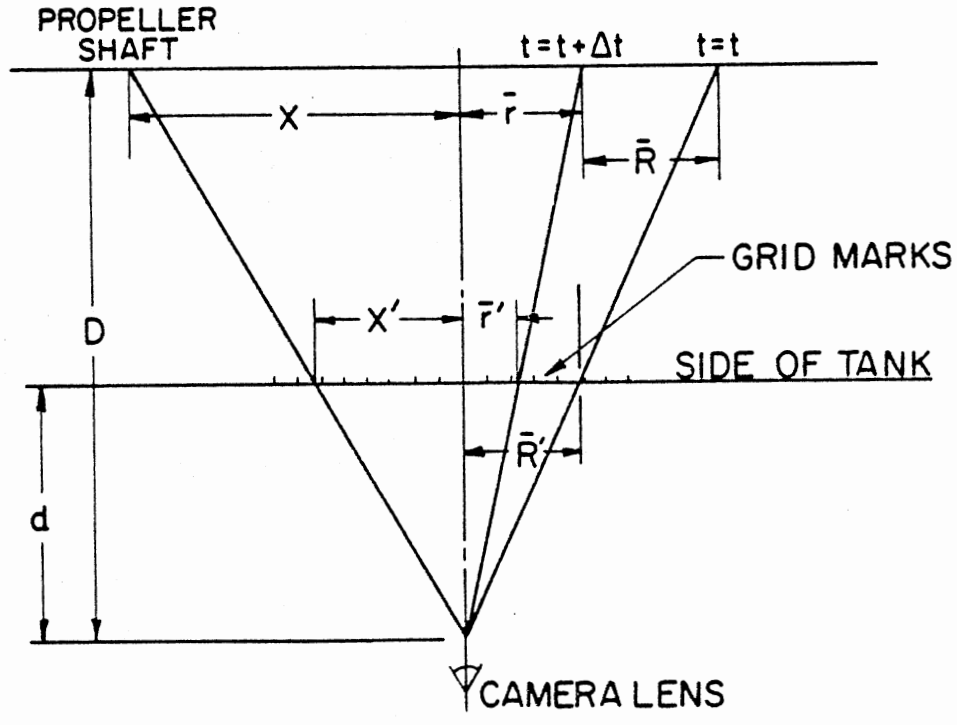

Figure 20. Drawing of the Flow Visualization Geometry [After Moon (14)]

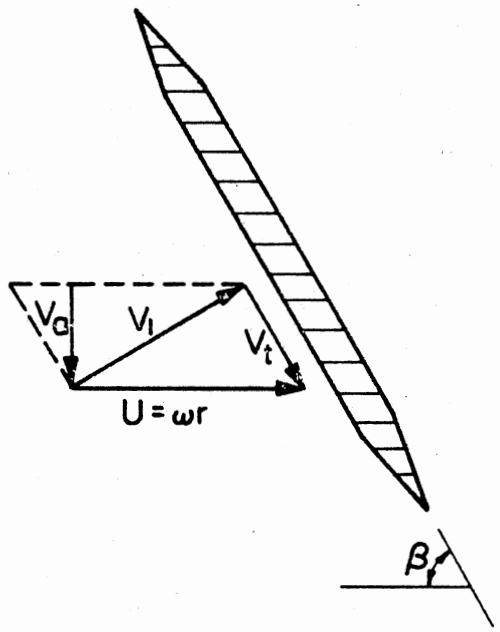

Figure 21. Vector Analysis of Flow Through a Propeller [After Moon (14)]

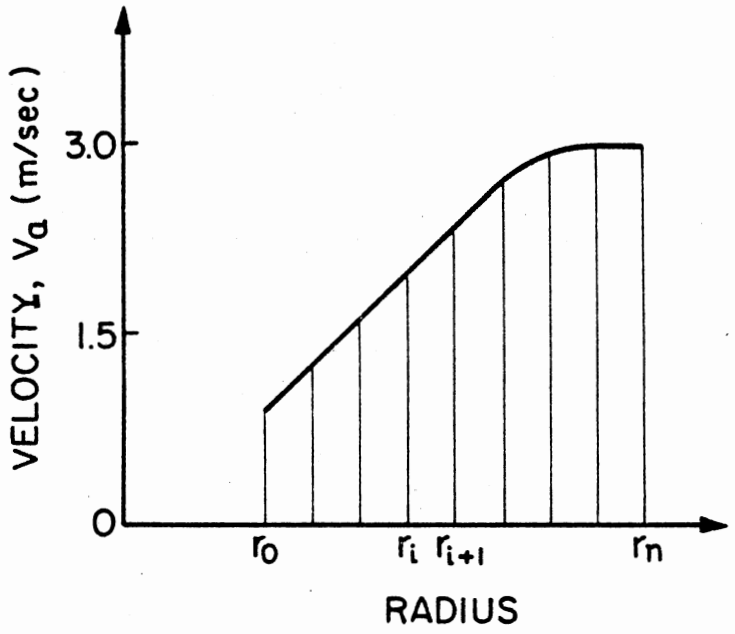

Figure 22. Axial Velocity, V_a, as a Function of the Radius, γ, for Constant Rotational Speed [After Moon (14)]

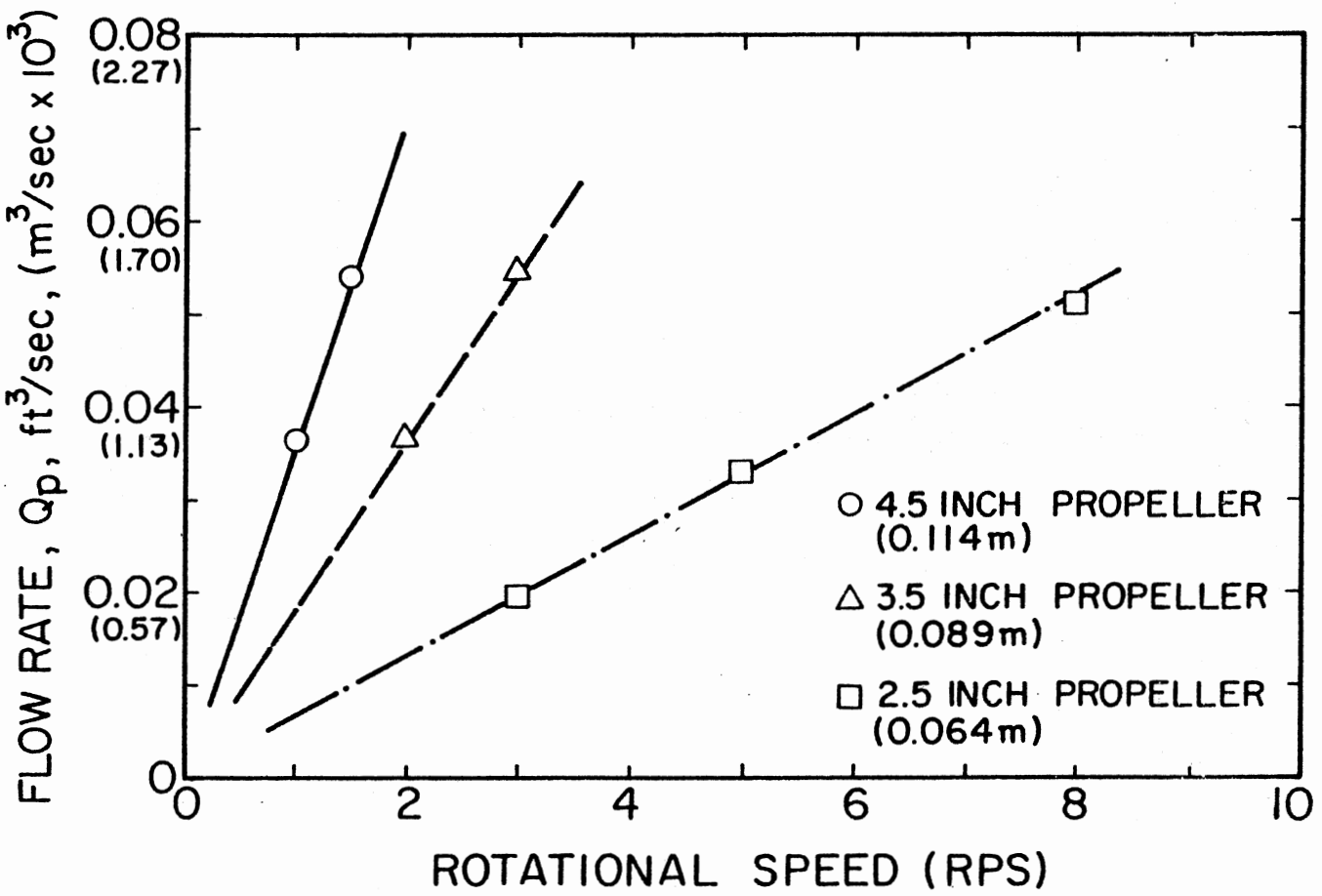

Figure 23. Propeller Calibration Using Flow Visualization [After Moon (14)]

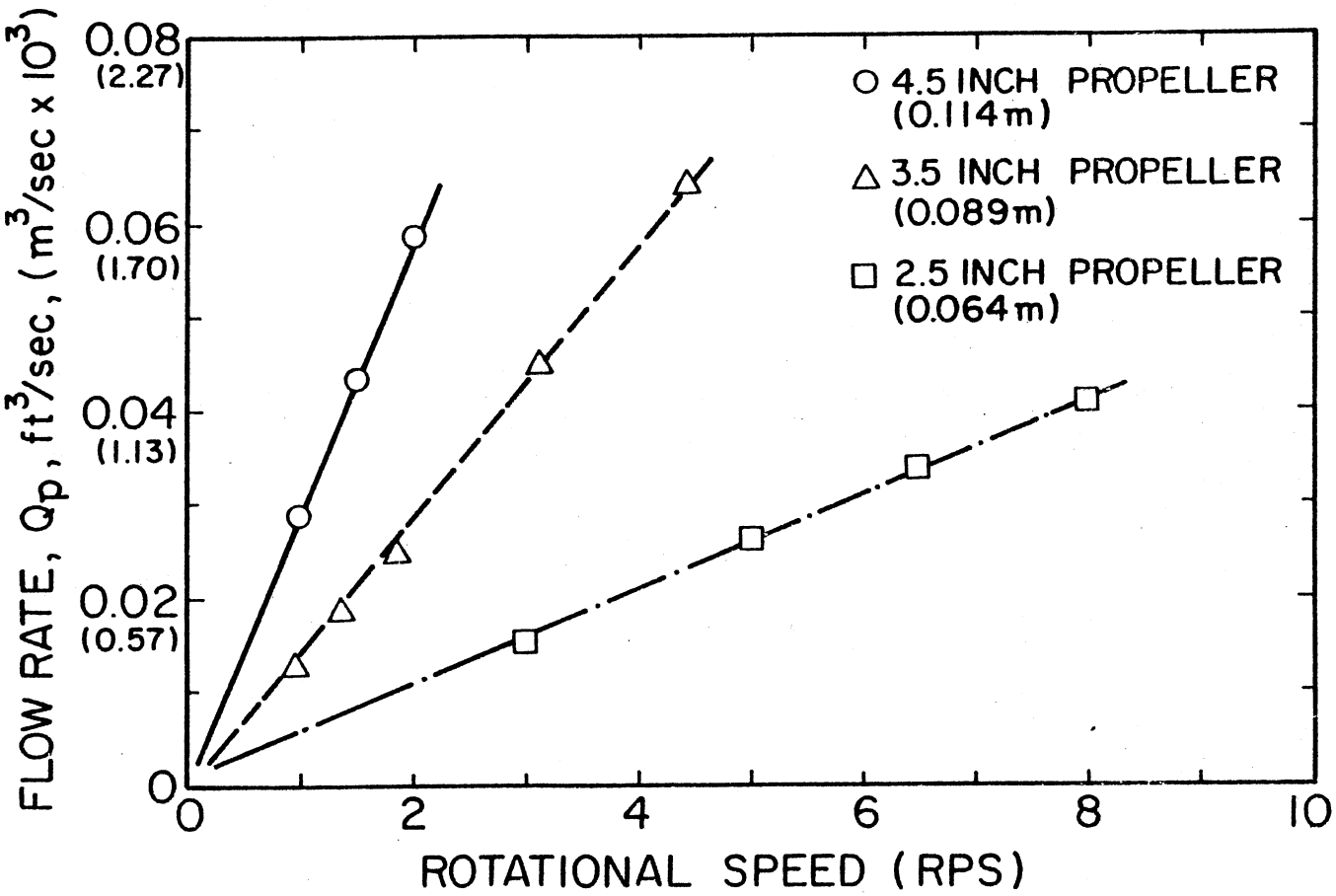

Figure 24. Propeller Calibration Using Vector Analysis [After Moon (14)]

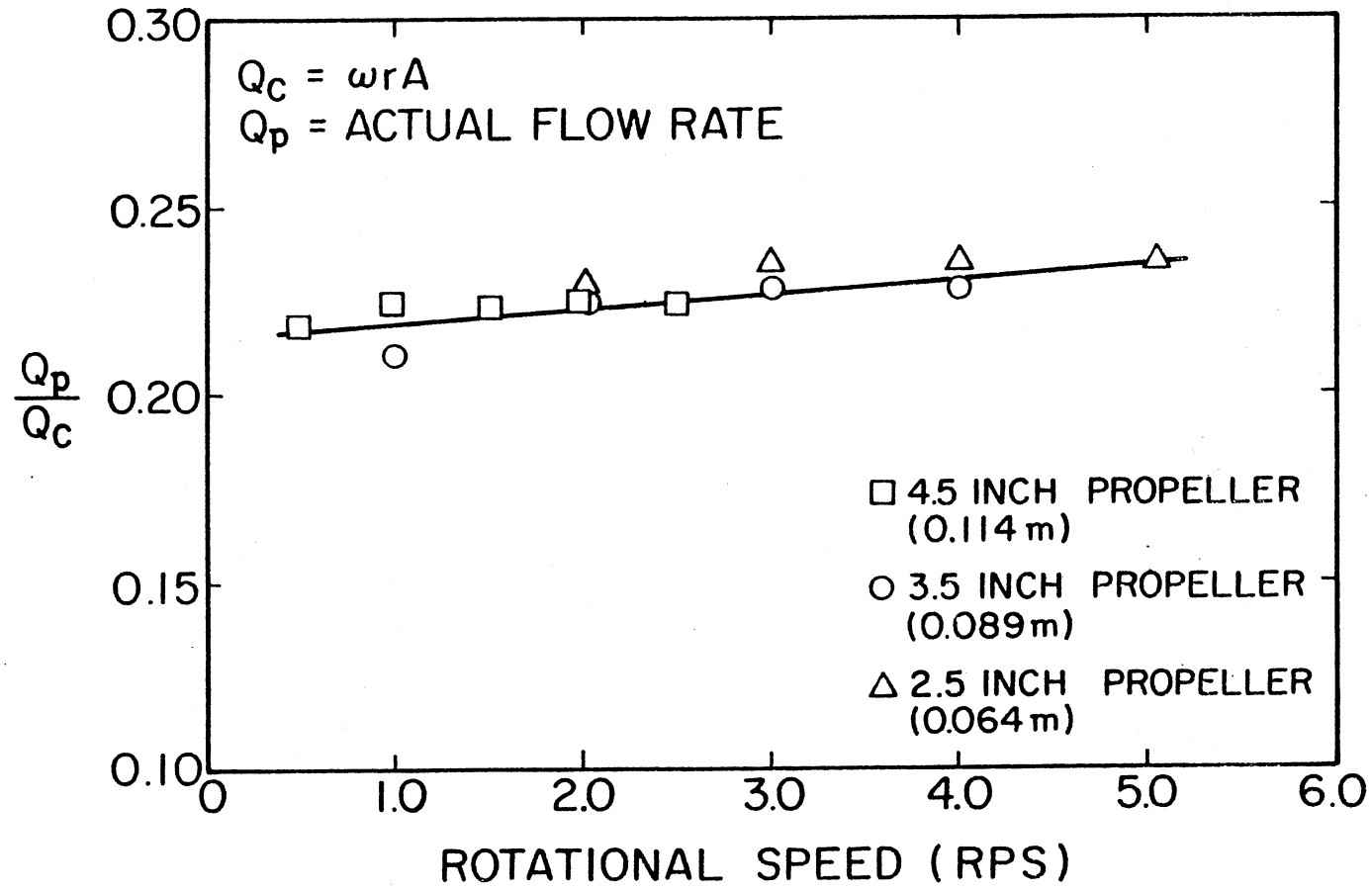

Figure 25. Normalized Flowrate, Q_p/Q_c as a Function of Rotational Speed [After Moon (14)]

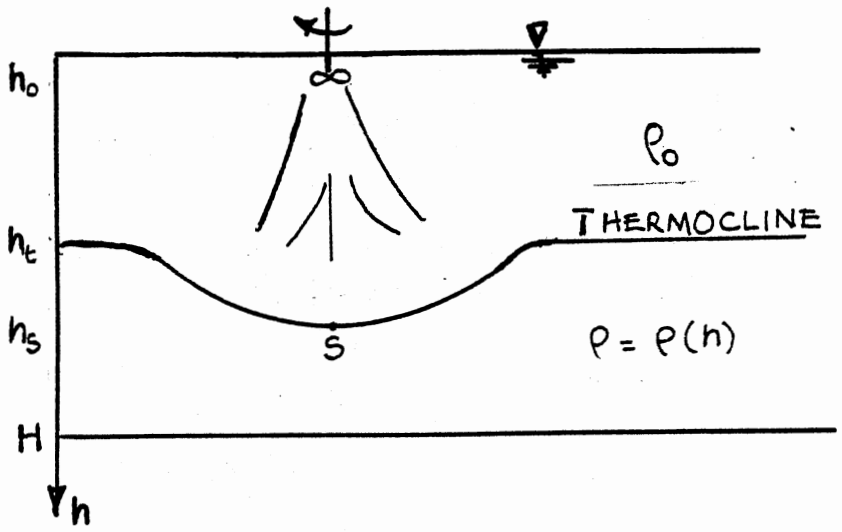

Figure 26. Propeller Jet Showing Important Parameters

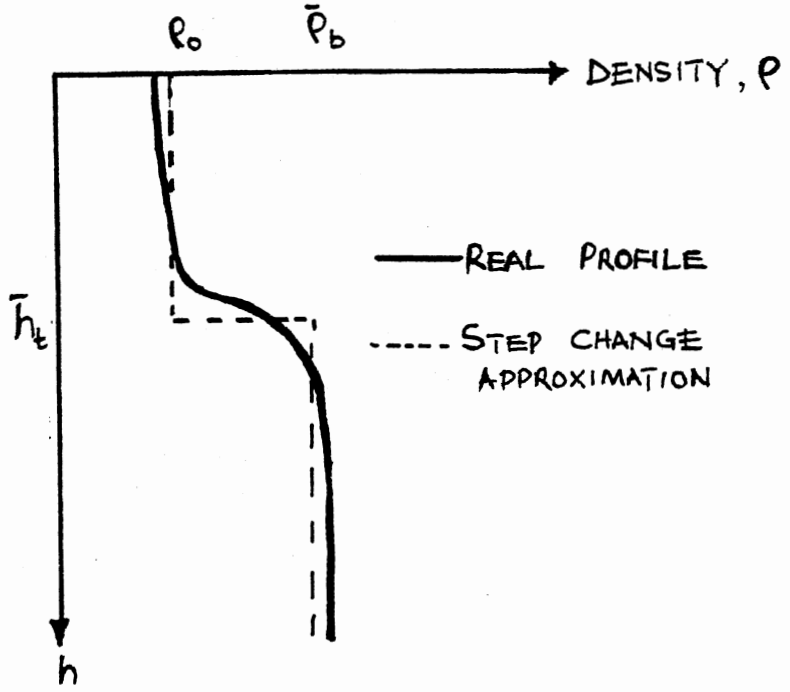

Figure 27. Actual and Theoritical Density Profiles

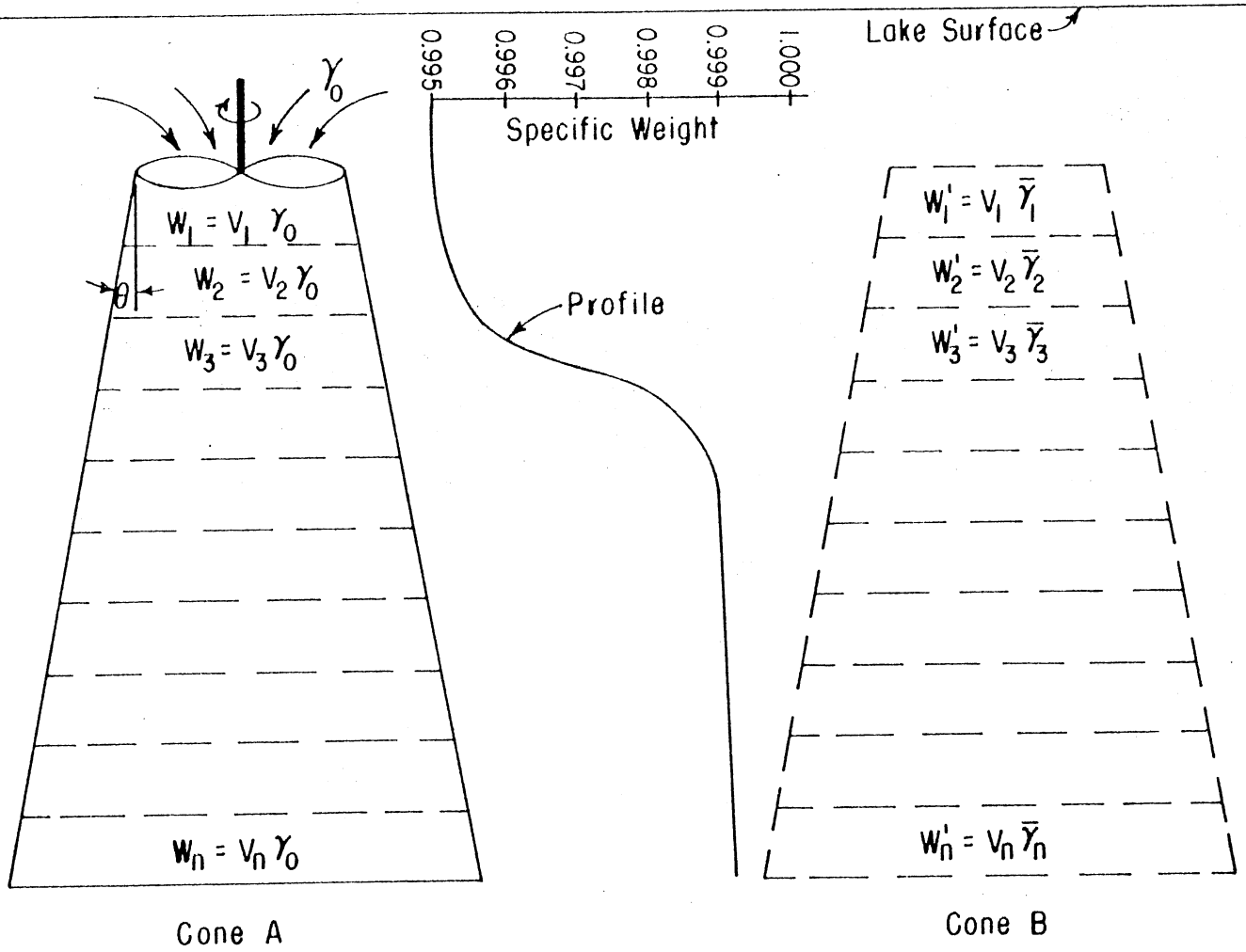

Figure 28. Depiction of Pump Plume [After Punnett (17)]

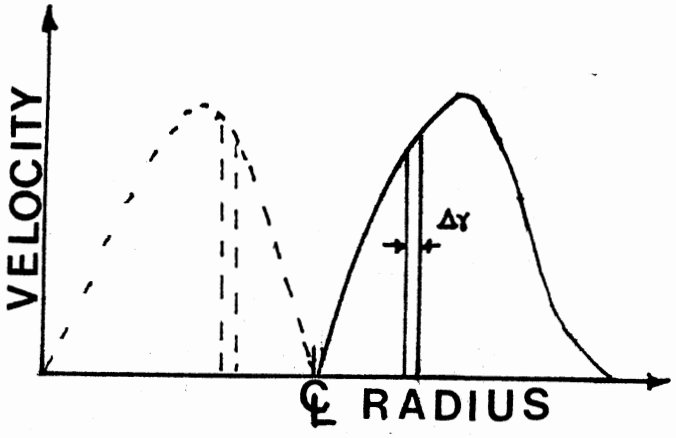

Figure 29. Local Velocity as a Function of Distance from Propeller Centerline

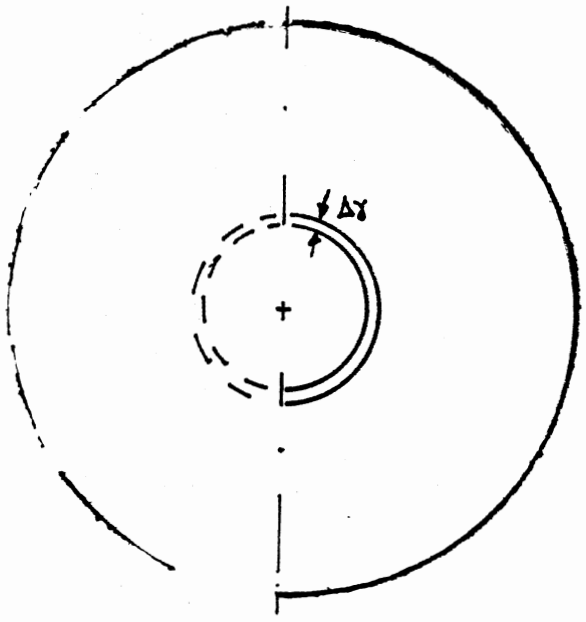

Figure 30. Typical Circle Showing Propeller Jet Area of Influence

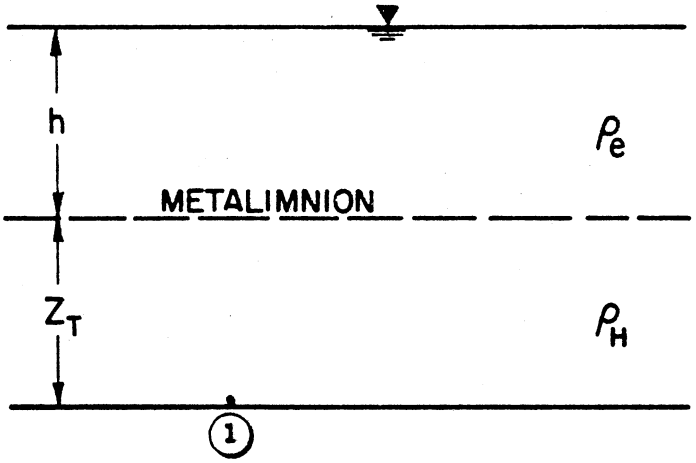

Figure 31. Stratification Without the Propeller Pump, Case I [After Moon (14)]

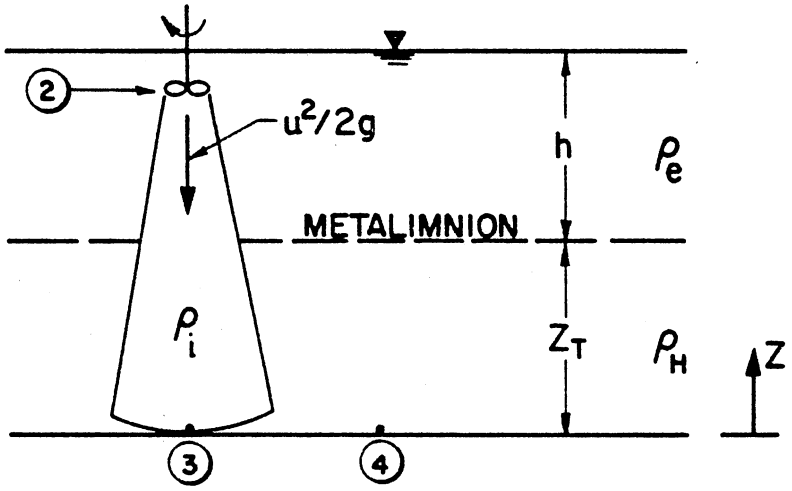

Figure 32. Stratification with the Propeller Pump, Case II [After Moon (14)]

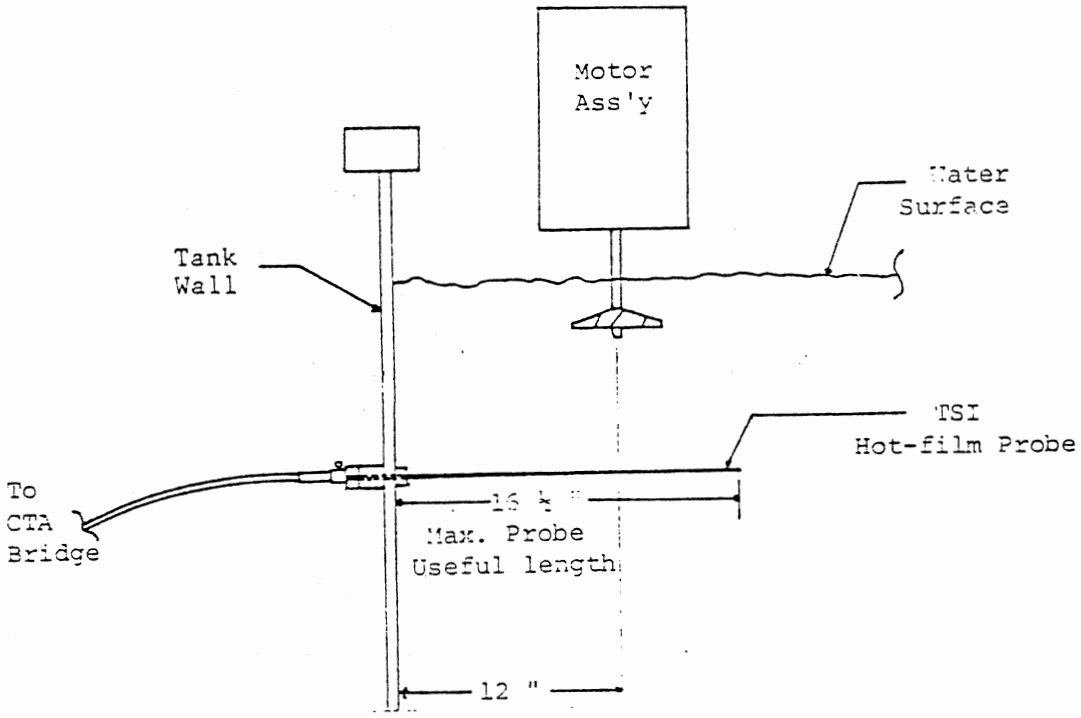

Figure 33. Schematic of Hot-film Probe Traversing Set-up Used by Haywood and Others

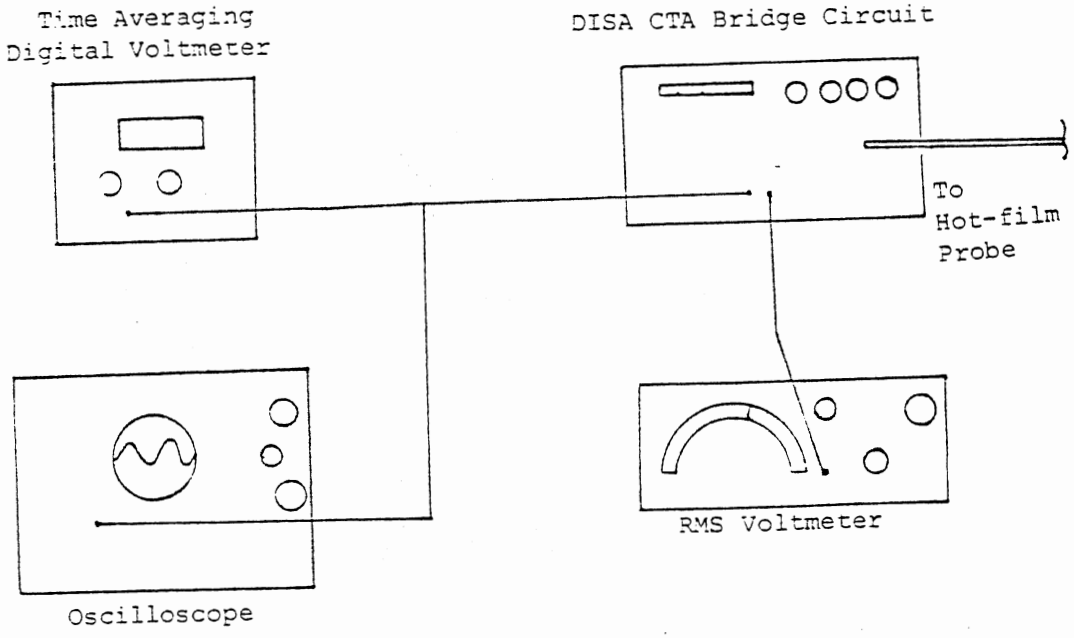

Figure 34. Schematic of Hot-film Probe Electronics Used by Haywood and Others

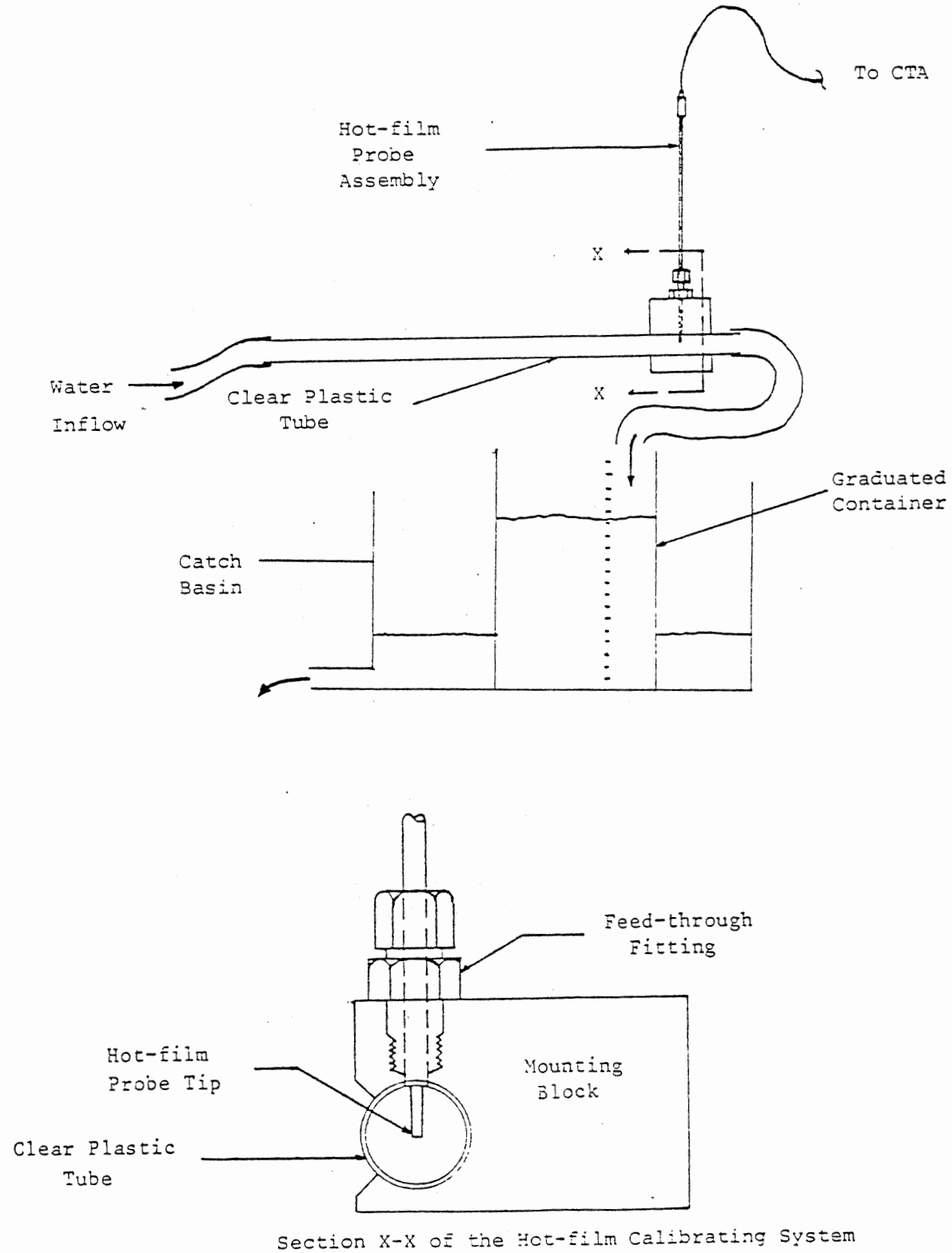

Figure 35. Schematic of the Hot-film Calibrating System Used by Haywood and Others

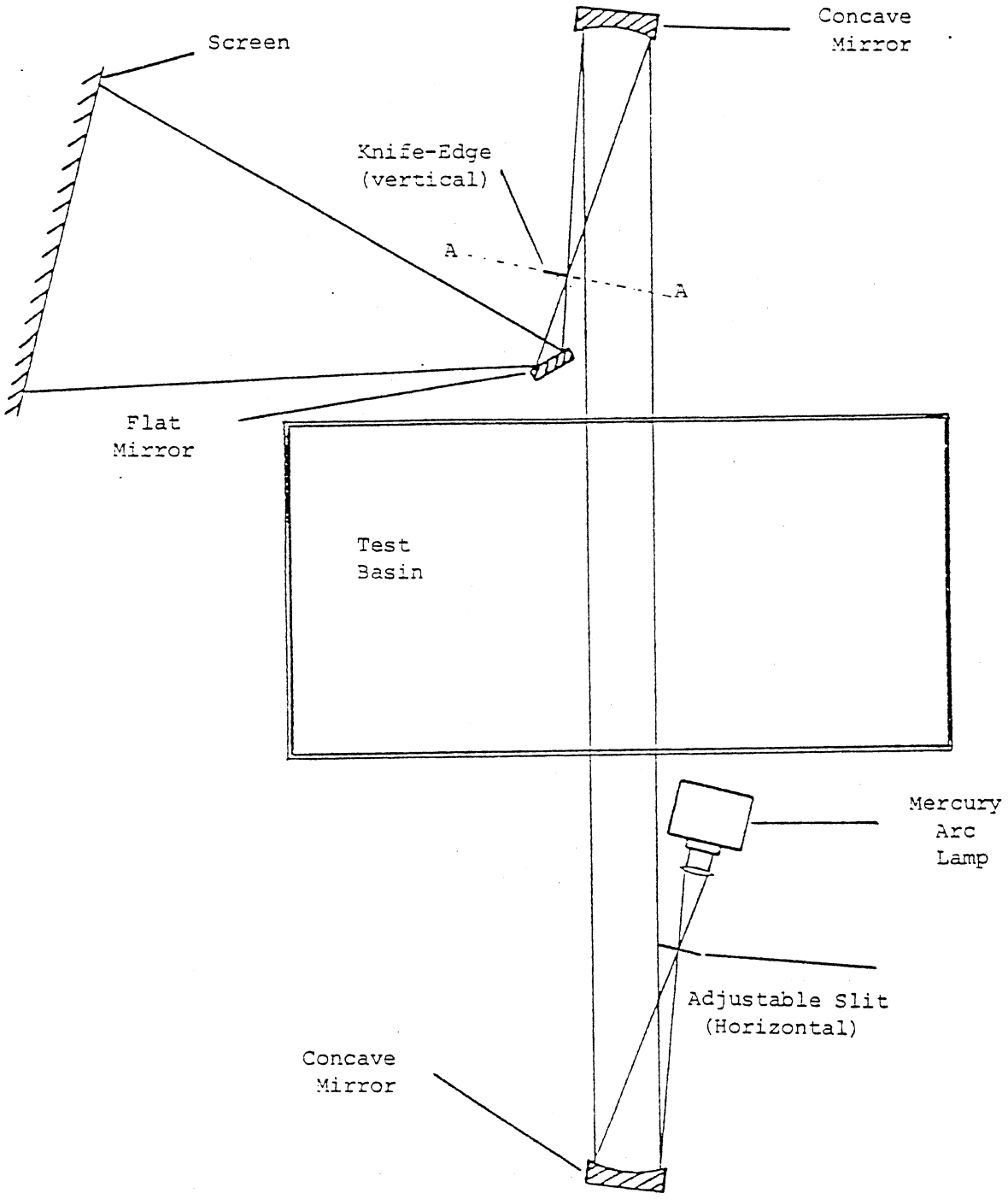

Figure 36. Schematic of the Schlieren Optics

APPENDIX B

PROPELLER CALIBRATIONS IN UNIFORM MEDIUM

Propeller Calibration

This is Moon's (14) analysis and procedures for calibrating the propeller in a uniform medium.

Propeller hydraulic modeling of the Garton propeller pump requires an accurate determination of flow rate as a function of rotational speed for each propeller model. The model flow rates scale with the prototype flowrate, where

$$\frac{Q_{pr}}{Q_m} = L_R^{5/2}$$

A plexiglass tank and a flow visualization technique were used to perform the calibrations. The flow visualization technique consisted of filming the displacement of a dye streak, due to the pumping of the propeller, over a time Δt using a 16 mm movie camera. From these data an accurate estimate of the propeller flow rate, Q_p, can be calculated. Figure 18 is a drawing representing the flow visualization.

The volume flow rate of the propeller pump, Q_p, is determined using a numerical integration scheme to find the volume of water displaced per unit time. (Figure 19)

$$Q_p = \frac{2\pi Lp}{t} \int_r^R r\,dt$$

$$Q_p = \frac{Lp}{\Delta t} (R^2 - r^2)$$

$$\text{or} \quad Q_p = \sum_{i=1}^{10} \frac{\pi (L_p/10)}{\Delta t} (R^2 - r_i^2)$$

where r_i is the distance from the dye streak to the center of the propeller shaft after an elapse time of Δt at the local vertical position

of Z. The initial distance of the dye streak to the center of the propeller shaft is represented by R. The finite differencing in the Z direction is done by measuring the average r at the ith location (see Figure 19).

The time, Δt, that elapses for a dye displacement of Δr is calculated from the camera speed (frames/second) and a frame counter on the projector.

The rotational speed of the propeller during the filming is determined from a period counter that is in the field of view of the camera. The signal to the period counter is supplied by a magnet causing a current to be indicated in a magnetic coil for each complete revolution of the propeller shaft.

Parallex calculations were performed to convert measurements from the film to actual measurements. The parallax correction equation are developed from the geometry of the system. Figure 19 is a drawing of the geometry.

$$X = X'(S/S_o)(D/d)$$

where

X = actual distance

X' = observed X from film

S_o = observed grid spacing from film

S = actual grid spacing (s = 2 in)

D = length from camera to propeller shaft, and

d = length from camera to side of tank.

Similarly,

$$\bar{r} = \bar{r}'\ (S/S_o)(D/d)$$

$$\bar{R} = \bar{R}'\ (S/S_o)(D/d)$$

$$r = \bar{r} + x$$

$$R = \bar{R} + x$$

where $\bar{R}$, $\bar{r}$ = actual distances;

$\bar{R}$, $\bar{r}'$ = observed, R, r from film.

R = distance from propeller shaft to dye streak at time = t; and

r = distance from propeller shaft to dye streak at time = $t + \Delta t$.

Calculations of flow rate, Q_p, as a function of rotational speed ω, were performed for each propeller. Using vector analysis (Figure 20). This theoritical flow rate is called Q_{pth}. Refering to Figure 21, it may be seen that

$$V_1 = U \sin \beta$$

$$V_a = V_1 \sin (90^o - \beta)$$

$$U = \omega r$$

Combining,

$$V_a = \omega r \sin \beta(\sin(90^o - \beta))$$

where

V_1 = normal velocity

V_a = axial velocity

U = velocity of a blade at radius = r;

ω = rotational speed; and

β = blade angle.

$$Q_{pth} = V_a A_p$$

Where A_p is the area of the propeller being considered, the value for the blade angle, β, varies as the propeller radius varies from r_{hub} to r_p. A different value for V_a was calculated for different values of T. As a result of these calculations, a plot of V_a as a

function of r was established (Figure 22). The theoretical flow rate, Q_{pth}, at a particular rotational speed, W, was calculated by numerically integrating the area under the curve shown in Figure 21, about the propeller circumference

$$Q_{pth} = \sum_{i=1}^{n} \pi \bar{V}_a (r_{i-1}^2 - r_i^2)$$

where

$$\bar{V}_a = (V_{a_i} + V_{a_{i-1}})/2$$

The calibration graphs for each propeller obtained from the flow visualization are presented in Figure 23. The calibration graphs for the propeller using the vector analysis are presented in Figure 24. Comparison of the two calibration plots reveals that the model propellers operate with an average efficiency, η, of 80 percent, where

$$\bar{\eta} = Q_p/Q_{pth}$$

Since each model propeller is a scale model of the 72 inch (1.83m) propeller used by Garton (10)(Figure 2), one would expect the normalized flow rates for each propeller at a given rotational speed to be equal. The normalization is achieved by dividing the propeller flow rate, Q_p, by an effective flow rate, Q_e.

$$Q_p/Q_e = Q_p/\omega r_p A_p$$

where

ω = rotational speed

r_p = propeller radius, and

A_p = area of the propeller.

The normalized flow rates, Q_p/Q_e, are represented in Figure 24 as a function of rotational speed, ω, for each model propeller.

The fact that the plot of Q_p/Q_e as a function of rotational speed (Figure 25) are approximately equal for each propeller gives an indication of the accuracy of the calibrations. It is estimated that the calibrations are accurate to within $\pm$ 5 percent of the values given in Figure 23.

APPENDIX C

PENETRATION DEPTH ANALYSIS

Penetration Depth Analysis

The penetration of the propeller jet can be approximately analyzed by applying Bernoulli's equation to the central streamline from the propeller plane (here considered as point o) and the stagnation point (point s) (Figure 26). The axial direction h is taken in the downward direction:

$$P_o + \frac{\rho_o V_o^2}{2} - \rho_o g h_o = P_s + \frac{\rho_o V_s^2}{2} - \rho_o g h_s \qquad \text{C-1}$$

ρ_o = epilimnion density

V_o = propeller induced central velocity

h_o = propeller depth

h_s = jet penetration depth

V_s = velocity at the stagnation point

The density in the last tern on the right is P_o because it can be assumed that the density throughout the jet $P = P_o$.

Since the velocity at the stagnation point is zero, Equation C-1 can be rearranged thus:

$$\frac{\rho_o V_o^2}{2} = (P_s - P_o) - \rho_o g (h_s - h_o) \qquad \text{C-2}$$

In the absence of strong currents below the stagnation point, it can be assumed that the pressure at the point s is the same everywhere in the basin at that level. Hence,

$$P_s - P_o = g\int_{h_o}^{h_s} \rho \, dh$$

$$= g\rho_o (h_s - h_o) + g\int_{h_o}^{h_s} (\rho - \rho_o) dh \qquad \text{C-3}$$

$\rho(h)$ is the stratification density as a function of depth. Putting C-3 into C-2 yields:

$$\frac{\rho_o V_o^2}{2} = g\rho_o (h_s - h_o) + g\int_{h_o}^{h_s} (\rho - \rho_o)dh - \rho_o g (h_s - h_o)$$

$$\frac{V_o^2}{2g} = \int_{h_o}^{h_s} \frac{\rho - \rho_o}{\rho_o} \, dh \qquad C\text{-}4$$

Since the epilimnion is well mixed the density is the same up to the thermocline and the integral in C-4 is approximately equal to zero from h_o to h_t. Hence the integral can be taken from h_t to h_s, giving

$$\frac{V_o^2}{2g} = \int_{h_t}^{h_s} \frac{\rho - \rho_o}{\rho_o} \, dh \qquad C\text{-}5$$

The interpretation of C-5 is that in a stratified medium the pressure is greater than the hydrostatic pressure that would arise due to the epilimnion density alone, by an amount (as a function of h):

$$P' = g\int_o^h (\rho - \rho_o)dh$$

The jet therefore penetrates to the depth at which stagnation pressure:

$$1/2\,\rho_o V_o^2 = P'$$

The real density profile of a stratified medium is as shown in Figure 27 (Full line) but it can be approximated by a step change as in the Figure (broken lines). The profile is described by a mean thermocline depth, h_t, and uniform densities above and below, P_o and $\bar{P}_b$;

$$\rho = \begin{cases} \rho_o \text{ for } h < \bar{h}_t \\ \rho_b \text{ for } h > \bar{h}_t \end{cases}$$

By this approximation C-4 can be re-written as:

$$\frac{V_o^2}{2g} = \int_o^{\bar{h}_t} \frac{\rho_o - \rho_o}{\rho_o} \, dh + \int_{\bar{h}_t}^{h_s} \frac{\rho_b - \rho_o}{\rho_o} \, dh$$

$$\frac{V_o^2}{2g} = \frac{\bar{\rho}_b - \rho_o}{\rho_o} (h_s - \bar{h}_t) \qquad \text{C-6}$$

An expression for the central velocity V(h) along the central axis of the jet, without considering the decay of jet as a result of viscous dissipation can be written as:

$$V(h) = V_o - \left(2g \int_{h_t}^{h} \frac{\bar{\rho}_b - \rho_o}{\rho_o} \, dh\right)^{1/2} \qquad \text{C-7}$$

In practice, V_o decreases with distance, h, and in the case of circular jets, V is inversely proportional to h (20) in a non-stratified medium.

$$V(h) = V_o \frac{KD_p}{h} \qquad \text{C-8}$$

D_p = propeller diameter

K = constant

Examination of C-8 shows that it is not valid for all h. For example for $h < KD_p$ the velocity is greater than V_o which is not possible.

A decay factor similar in behavior to 1/h and which applies for h KD_p is exp $(-Kh/D_p)$.

The central velocity expression now becomes

$$V(h) = V_o \exp\ (-Kh/d_p) - (2g \int_{\bar{h}_t}^{h} \frac{\bar{\rho}_b - \rho_o}{\rho_o})^{1/2} \qquad C\text{-}9$$

At stagnation point $h - h_s$ and $V(h_s) = 0$, hence

$$\frac{V_o^2}{2g} \exp\ (-Kh_s/D_p) = \frac{\bar{\rho}_b - \rho_o}{\rho_o} (h_s - \bar{h}_t) \qquad C\text{-}10a$$

or

$$\frac{V_o^2}{2g} \exp\ (-Kh_s/D_p) = (\Delta\rho/\rho_o)\Delta\bar{h}_{st} \qquad C\text{-}10b$$

In selecting the decay factor it has been assumed that the density gradient due to stratification will not have any effect on its behavior.

Prediction of Penetration
After Punnett (17)

A method of predicting the maximum depth of penetration was developed by Dr. James Garton (unpublished). As surface waters are pumped by a single unit at a low velocity downward into denser waters, a conical plume of water having a nearly uniform specific weight, δ_o, is formed. Cone A in Figure 28 represents this plume. It is assumed the specific weight of the water in the plume is the same as the water at the impeller level of the pump. Cone B (Figure 28) represents the volume of water displaced by Cone A. The varying specific weight of the water in Cone B is dependent upon the density profile of the lake.

Each cone is divided into one m slices, forming frustums, and the volume for each is calculated for a given angle of entrainment, θ. For Cone B, an average specific weight, δ_o, is calculated for each frustum. The weight of each frustum is determined by multiplying the volume

times the specific weight. The total weight of each cone is found by summing the weights of the frustums. Cone A, being less dense, will weigh less than Cone B.

According to Archimedes' principle, there is a buoyant force acting on Cone A equal to the weight difference of Cones A and B. The pumping force required to maintain Cone A (e.g. to displace Cone B) is equal to, and opposite, the buoyant force. Thus,

$$F_R = W_A - W_B;$$

where

F_R = pumping force required

W_A = weight of Cone A

W_B = weight of Cone B

The predicted depth of penetration is the depth at which the total pumping force supplied is equal to the pumping force required to maintain the plume geometry.

Since the centroid of each frustum is slightly lower than the midpoint, a "weighted" average specific weight is desirable. Using the equation for the volume of a frustum, and multiplying the upper and lower surface times the appropriate specific weight, the following equation was developed to yield a "weighted" slice weight:

$$W = 1/3\ h\ (\delta_1 B_1 + \delta_1^2 B_2 + \sqrt{B_1 B_2 \delta_1 \delta_2}\ ;$$

W = weight of frustum

h = height of frustum

B_1 = upper surface area

B_2 = lower surface area

δ_1 = specific weight of B_1

δ_2 = specific weight of B_2

The arrangement of the pump(s) determines the plume geometry. For a conical plume (e.g. a single pump), the frustum surface areas, B_1 and B_2, are found by calculating the area of a circle. For a square (or rectangular) cluster of pumps, the frustum surface area are assumed to be square (or rectangular).

The penetration was calculated using a computer program. By supplying the impeller depth, shape of the plume, side length(s) (or diameter), angle entrainment, pump flow rate per pump, average velocity of flow through the impeller, number of pumps, and a temperature profile having one m intervals the depth of penetration is predicted.

Measurement of the Cone Angle

As the flow of water passed through the impeller a natural divergence, or angle of entrainment, began. Establishment of the angle of entrainment was necessary so that plume volume calculations could be made. By lowering a water quality probe down at a known horizontal distance from the impeller, the cone of influence could be detected by variable temperature, oxygen and conductivity readings. Knowing the vertical distance lowered from the impeller depth and the horizontal distance from impeller, the cone angle could be determined by using trigonometric relationships.

Penetration Depth Analysis
After Moon (14)

This section presents the derivation of the following equation,

$$u^2/2g = (\Delta\rho / \rho_o) Z_T$$

where

u = average axial velocity;

$\Delta\rho/\rho_o$ = stratification; and

Z_T = height of the metalimnion.

The equation shown above states that the velocity head, $u^2/2g$, required to displace the metalimnion to the bottom of the system (i.e., $Z_T = 0$) is approximately equal to $(\Delta\rho/\rho_o)Z_T$ for a step density profile.

Case I

From Bernouilli's equation (see Figure 31),

$$P_{T1} = (\rho_e + \Delta\rho)gZ_T + \rho_e gh$$

where $\rho_H = \rho_e + \Delta_p$.

Case II

Figure 32 is a sketch representing this derivation. From Bernouilli's equation,

$$P_{T2} = P_3 + 1/2\rho u_3^2 + gZ_3$$

When the jet is penetrating to the bottom of the stream (i.e., point 3), $u_3 = 0$, $Z_3 = 0$. Therefore,

$$P_{T2} = P_3$$

The pressure inside the jet at the stagnation point is equal to the pressure outside the jet. Therefore,

$$P_3 = P_4$$

Consequently,

$$P_{T2} = P_4$$

But P_4 can be calculated from Case I.

$$P_4 = (\rho_e + \Delta\rho)gZ_T + \rho_e gh$$

Also,

$$P_4 = P_3 + 1/2\,\rho u_3^2 + \rho g Z_3 = P_1$$

Since P_1 for Case I equals P_4 for Case II, then,

$$\rho_e gh + (\rho_e + \Delta\rho)gZ_T = \rho_i gh + \frac{1}{2}\,\rho_i u^2 + \rho_1 gZ_T$$

where

$$\rho_i = \rho_e$$

ρ_i = density inside the jet

$$\rho_e gh + (\rho_e + \Delta_p)gZ_T = \rho_e gh + \frac{1}{2}\rho_e u^2 + \rho_e gZ_T$$

Therefore,

$$u^2/2g = (\Delta\rho/\rho_e)Z_T$$

APPENDIX D

AVERAGE VELOCITY CALCULATIONS

"Average Velocity" Calculation

The steps involved in the calculation of the propeller average velocity are as follows:

(1) Convert the pressure measurements at points along the propeller diameter to local velocity measurements.

(2) Convert the local velocity measurements to local volume flow measurements.

(3) Divide the sum of the volume flows by the sum of the local cross-sectional areas to get the average velocity.

Pressure Measurements Conversion

From the pressure profile diagram (Figure 11) the average pressure at each radius is obtained by calculating the average of the readings obtained for the radius, left and right of the propeller shaft center line. A plot of such average pressure against the radius is shown in Figure 29.

Using Bernoullis equation the pressure readings at each radius is obtained thus:

$$\frac{g_c}{g}\frac{P_1}{\rho} + \frac{\bar{V}_1^2}{2g} = \frac{g_c}{g}\frac{P_2}{\rho} + \frac{\bar{V}_2^2}{2g} \qquad \text{D-1}$$

Point 1 is the point under the propeller while point 2 is the quiet part of the basin. Points 1 and 2 are of the same vertical height. The unit of each of the terms in D-1 is length (head). The first term on each side of the equality is the static pressure head while the second is the velocity head.

Rearranging equation D-1 ($\bar{V}_2 = 0$), we have

$$V_1 = \sqrt{\frac{2g_c \Delta_p}{\rho}} \qquad \text{D-2}$$

P is measured in inches of water hence,

$$V_1 = \sqrt{\left[2 \times \Delta P \text{ (in of water)} \times \frac{5.195 \text{ lb}_f/\text{ft}^2}{\text{in of water}} \times 32.174 \frac{\text{lbm}}{\text{lb}_f} \right.}$$

$$\left. \frac{\text{ft}}{\text{sec}^2} \times \frac{\text{ft}^3}{62.4 \text{ lbm}} \right]$$

$$V_1 = 2.31 \sqrt{\Delta P} \text{ ft/sec} \qquad \text{D-3}$$

With the relationship of D-3 the local velocity is obtained for each radius.

Local Velocity Conversion

A circle representing the area the influence of the jet at the level under consideration is drawn. The radius of the circle is the distance cut in by the curve on the radius axis. Next the circle is divided into rings, $\Delta \gamma$ apart corresponding to the division in Figure 29. This means that each ring is associated with a partition on the curve.

Multiplying each local velocity with its corresponding area gives the local volume flow through the cross section.

Local Volume Flow at $\gamma_\eta = V\gamma_\eta \times 2\pi\gamma_\eta\Delta\gamma$ D-4

V is the local velocity at γ_η

Analyzing D-4 further, we have

$$V\gamma_\eta \times 2\pi\gamma_\eta\Delta\gamma = V\gamma_\eta \times \pi \left[\left(\gamma_\eta + \frac{\Delta\gamma}{2}\right)^2 - \left(\gamma_\eta - \frac{\Delta\gamma}{2}\right)^2\right] \qquad \text{D-5}$$

The total volume flow is the sum of the values obtained with D-5, and dividing this by the sum of the cross-sectional areas give the "Average velocity."

$$\text{Total Volume Flow} = \sum_{1}^{n} \gamma_n \quad \pi \left(\left(\gamma_n + \frac{\Delta_\gamma}{2} \right)^2 - \left(\gamma_n - \frac{\Delta_\gamma}{2} \right)^2 \right) \qquad \text{D-6}$$

$$\text{Total Cross-Sectional Area} = \sum_{1}^{n} \pi \left(\left(\gamma_n + \frac{\Delta\gamma}{2} \right)^2 - \left(\gamma_n - \frac{\Delta\gamma}{2} \right)^2 \right) \qquad \text{D-7}$$

$$\text{Average Velocity} = \frac{\Sigma \text{ Volume Flow}}{\Sigma \text{ Area}} \qquad \text{D-8}$$

APPENDIX E

SUMMARY OF EXPERIMENTS BY HAYWOOD AND OTHERS

Summary of Experiments

In addition to most of the apparatus used for the test in the body of the thesis, the hot-film anemometer equipment and the schlieren optical equipment were used.

The propeller equipment was modified such that the propeller rotation was monitored by an optical limit switch sensing unit that contained an infrared light emitting device (LED) and the detector. A disk with sixty holes on its periphery was mounted on the propeller shaft so that it spun between the light source and the dector. The pulse train produced was fed into a frequency counter which converted rotational speed into revolutions per minute.

A constant - temperature anemometer (CTA) was used to measure the velocity at several points in the propeller flow field. A hot-film probe was connected to an oscilloscope, a time averaging digital voltmeter, and a voltmeter (Figures 33 to 35).

Light from a slit source (a mecury arc lamp) was focused in the center of the test section of the basin. After passing through the tank the light was re-focused on a knife-edge. The light not intercepted by the knife-edge was turned ninety degrees by a small first surface mirror to project the image of the test section on a screen for viewing and photograph (Figure 36).

Dye Visualization

After stratifying the tank and verifying its density profile, flow visualization and velocity measurement tests could be performed. The procedure for performing dye visualization tests started with choosing

a propeller depth and speed. The propeller drive assembly was raised or lowered to the desired position and the drive motor supply voltage preset to the approximate value to obtain the desired speed (the voltage/speed relation was previously determined). To start a run, the propeller drive motor was started and minor adjustments in supply voltage quickly made to set the speed to the desired value. Next, the dye flow and the movie camera were started simultaneously and allowed to run until the dye had penetrated to its maximum depth for about five seconds. At this point, the motor and dye flow were stopped, but the camera was left running to record the thickness of the dye-laden metalimnion layer, or "lens". After the tank was allowed to settle for twenty to thirty minutes, another density profile was taken to check the degradation of the thermocline. If the profile was still satisfactory, another run could be made. Usually, only two runs could be carried out before the tank had to be drained and restratified.

Schlieren Flow Visualization

Since schlieren flow visualization depends upon the presence of density gradients in the flow field, it is only useful in the stratified tests, where the large fresh water/salt water density difference provided excellent contrast. Setup for the schlieren optics consisted of placing the source, mirrors, and knife-edge in the proper positions (see Figure 36)at the desired depth to observe the jet stagnation point, and then very carefully adjusting the light path. The mirror distances were first adjusted to achieve a constant-diameter light beam through the test section, then the mirror angles were arranged to make the light beam perpendicular to the sides of the tank and parallel to the

plane of the metalimnion. The latter adjustment was especially important when the metalimnion was centered in the light beam, to prevent excessive refraction, which spreads the image of the interface into a wide, dark band. Depending on the sharpness of the density gradient, the dark band could not always be narrowed satisfactorily. The next adjustment made was the knife-edge positioning. If the knife-edge is not positioned properly at the image plane (A-A), the system will operate as a shadowgraph instead of a schlieren, and the image contrast will be decreased markedly. Photography was done with both 35-mm reflex and 16-mm movie cameras. Due to the very dim output of the schlieren system, the film used (400 and 200 ASA for the reflex and movie cameras, respectively) required a special developer to raise the effective ASA number and enhance the underexposed images. Normal printing procedures were then used to produce the 35-mm prints.

Velocity Calibration

Measurements of jet axial velocity were carried out by traversing the hot-film probe across the jet at several depths beneath the propeller. Before each use of the hot-film system, it was calibrated in an apparatus designed and built especially for the purpose (Figure 35). The system was adjusted for optimum frequency response before calibration and again after installing the probe in the tank wall, to adjust for any differences in water temperature between the calibrating stand and the tank so that the same overheat ratio was maintained. Then, starting two inches from the wall, measurements of probe voltage for the mean and the fluctuating velocity components were taken at

intervals across the jet under the propeller.

RESULTS AND DISCUSSION

Dye Visualization

Films taken of dye runs were useful as a record of jet behavior under various conditions, but when measurements of penetration were taken off of the films the results were not accurate. This was due to the differing geometries between runs and could be corrected by careful setup and noting of geometry. Because of the inaccuracies of the filming process and the long time required for film processing, dye visualization penetration measurements were made visually with adequate precision. Figure 18 shows the relationship between jet penetration into the thermocline and separation distance of the propeller and the thermocline.

Schlieren Flow Visualization

Schlieren optical techniques are commonly used in flow situations in which density gradients are produced in a homogeneous medium by compressibility effects or temperature differences. Preliminary tests of a simple schlieren system in this application have shown great potential for high-resolution visualization of penetration depth and turbulence in the pump plume. The large density difference between the fresh and salt water made for excellent contrast at the edge of the plume.

Aside from clear definition of the pump plume boundaries, the major advantage of the schlieren in this application is the absence of

parallax due to the parallel light path through the test section. This facilitated penetration depth measurements since no correction for camera distance and angles were required. As long as an accurate scale is marked on the tank wall, distances may be measured directly on the screen or on a photograph and then scaled linearly by the ratio of actual test section size to image size.

The schlieren has several major disadvantages which must be weighed against the good qualities mentioned above. One of these is the necessity of precise alignment of the optics. The aligning procedure increases the setup time required for an experiment, and any accidental movement of a mirror may entail time-consuming readjustment. The low light output of the system is also a problem, requiring working in near total darkness and special film processing to bring out the underdeveloped images. The major problem, however, is the limited field of view allowed by the mirrors used. This made it impossible to view more than a small portion of the plume, and thus very difficult to catch the point of maximum penetration. The only solution for this problem would be to use larger mirrors, which would probably be very expensive.

Hot-film Measurements

The general shape of the velocity profile of the jet has been previously confirmed to have a maximum on either side of the center of the cross-section of the jet, and a minimum at the center indicating the wake of the propeller shaft. The hot-film method yielded similar results, except that its performance deteriorated rapidly as turbulence in the jet increased. The profile shape developed anomalies as the

propeller shaft speed increased, therefore, as the turbulence increased, for both the free jet and the jet with a flat plate obstruction placed 2.61 diameters below the propeller.

As the jet is examined at points further and further away from the propeller, it would be expected to be dispersed by the resistance of the more stationary water around it, and therefore to be more turbulent at greater distances from the propeller. The hot-film method loses credibility in turbulent situations. The profile taken at a distance of two propeller diameters is extremely mis-shapen, while that taken at one diameter has the expected shape and can be assumed to be a much more accurate representation of its situation.

The reason for the poor performance of the hot-film probe in turbulent situations is in the shape of the hot-film element itself. It is long enough that it cannot provide correct measurements of three-dimensional flows. Accurate measurements can be obtained only if the flow is perpendicular to the axis of the element. Apparently, as the propeller speed is increased or the downstream distance at which measurements are taken is increased, the jet's lateral turbulence increases enough to give the flow velocity a significant component parallel to the axis of the hot-film element. This would cause variations of the type that occurred.

CONCLUSIONS

I. Dye visualization proved to be of value in getting an overall view of the penetration and mixing processes, and of the lensing effect in the metalimnion. Motion-picture filming of the dye penetration proved too inconsistent for quantitative analysis, but visual measurement

techniques were successful.

II. Schlieren optical techniques were shown to be practical for observing local destratification phenomena. Major advantages noted were the ability to obtain clear definition and precise location of plume boundaries. Disadvantages included narrow field of view, long setup times, and low light output, but these problems could be eliminated through further refinement of the system.

III. Use of hot-film anemometry to measure velocities in propeller jets is extremely difficult due to the highly turbulent nature of the flow field. Measurements taken of velocity profiles across jets under various conditions showed general trends, but quantitative analysis of the data yielded highly uncertain results.

IV. Jet penetration decreases as the distance between the propeller and the metalimnion is decreased for distances less than about two propeller diameters and as the propeller metalimnion distance is increased above two propeller diameters.

VITA[2]

Howells Idaerefagha Hart

Candidate for the Degree of

Master of Science

Thesis: JET PENETRATION DEPTH MEASUREMENTS AND AXIAL-FLOW PROPELLER PUMP RE-CALIBRATION IN A STRATIFIED MEDIUM

Major Field: Mechanical Engineering

Bibliographical:

Personal Data: Born in Bonny Town, Nigeria, February 13, 1951, the son of Mr. and Mrs. E. B. Hart.

Education: Attended Ngwa High School, Aba, Nigeria and obtained the University of London General Certificate of Education in January 1971; received the Bachelor of Engineering degree from the University of Benin, Benin-City, Nigeria in February, 1977; trained in Power System Maintenance at AB electro-Invest, Stockholm, Asea AB, Vasteras and AB Hedemora Verkstader, Hedomora, Sweden in 1979; completed requirements for the Master of Science degree at Oklahoma State University in July, 1981.

Professional Experience: Youth Service Corps Engineer, Yola, Nigeria, 1976-1977; Mechanical Engineer, Ministry of works, Port -Harcourt, Nigeria, 1977-1978; Executive Engineer, Secretariat Complex Engineering facilities, Governor's office, Port -Harcourt, Nigeria, 1979-1980; graduate research assistant, Department of Mechanical and Aerospace Engineering, Oklahoma State University, 1980; graduate teaching assistant, Department of Mechanical and Aerospace Engineering, Oklahoma State University, 1981.

Professional Societies: American Society of Heating, Refrigeration and Air-Conditioning Engineers.